AD-A085 968 NATIONAL AERONAUTICS AND SPACE ADMINISTRATION HAMPTO--ETC F/G 20/4
DEVELOPMENT AND VALIDATION OF A COMBINED ROTOR-FUSELAGE INDUCED--ETC(U)
JUN 80 C E FREEMAN

UNCLASSIFIED NASA-L-13363 NASA-TP-1656 NL

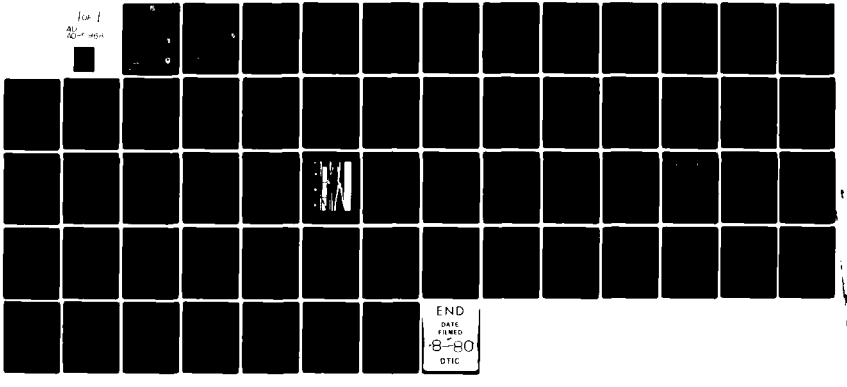

END
DATE FILMED
8-80
DTIC

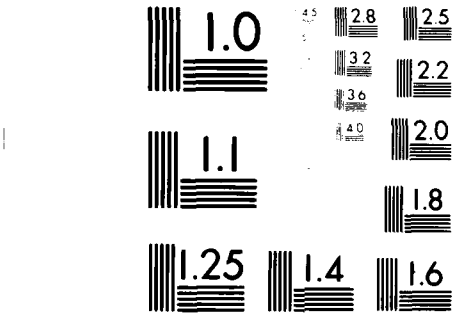

NASA Technical Paper 1656

AVRADCOM Technical Report 80-B-3

(19) NASA-L-19363

Development and Validation of a Combined Rotor-Fuselage Induced Flow-Field Computational Method

(18) NASA / USAAVRADCOM

(17) TP-1656 / TR-80-B-3

(10) Carl E. Freeman

(11) January 1980

(12) 61

NASA
Technical Paper 1656

AVRADCOM
Technical Report 80-B-3

Development and Validation of a Combined Rotor-Fuselage Induced Flow-Field Computational Method

Carl E. Freeman
Structures Laboratory
AVRADCOM Research and Technology Laboratories
Langley Research Center
Hampton, Virginia

National Aeronautics
and Space Administration

Scientific and Technical Information Office

1980

SUMMARY

A potential-flow panel method has been modified to calculate the effects of a rotor wake on the time-averaged surface pressure and velocity distributions on a helicopter fuselage. The rotor-induced velocities are calculated by using a vortex-tube wake model. The calculated pressure distributions are found to compare well with experimental data obtained from tests of a wind-tunnel model.

INTRODUCTION

The fuselage of a helicopter operates in a flow field which is composed of a combination of its forward flight velocity and the downwash induced by the rotor system. This combination can range from only the rotor-induced field at hover to very little rotor downwash effect at high speeds. Analysis of this flow field at any condition from hover to high-speed flight is important in designing the fuselage and its various components (such as wings and tails).

Potential-flow panel methods (ref. 1), which use source and/or doublet panels to model rather complex vehicles, have been developed to analyze the flow field of fixed-wing aircraft. Much work (refs. 2 to 12) has been done in the helicopter community to analyze the induced flow of a rotor system. These methods range from simple actuator disk theory to unsteady lifting-surface methods.

Even though the dynamic nature of the rotor wake is important in analyzing certain problems such as vibration, many design details can be analyzed by using a time-averaged downwash field. Therefore a computer code has been developed to combine a vortex-tube rotor-wake theory with an incompressible, potential-flow panel method. This method calculates both on-body and off-body velocities, fuselage surface pressures, and total loads.

This paper includes a discussion of the basic theories, which are incorporated in the present computer code, with a general description of the computer code and the experimental test, which was used as a basis for validation. Experimental fuselage surface pressure data were obtained from a helicopter wind-tunnel model at an advance ratio of 0.05. Comparisons of experimental data and the analytical method are presented for thrust coefficients of 0.0034, 0.0050, 0.0066, and 0.0082.

SYMBOLS

Units used for physical quantities defined in this paper are given in the International System of Units (SI). The positive senses of parameters are shown in figure 1.

a_0	coning angle, deg
a_{1s}	first-harmonic rotor longitudinal flapping angle, deg
A	rotor-wake cross-section area, m^2
A_1	lateral cyclic control, deg
b_{1s}	first-harmonic rotor lateral flapping angle, deg
B_1	longitudinal cyclic control, deg
$C_1,\ldots,C_8$	constants defined in equation (37)
C_p	pressure coefficient
C_T	rotor thrust coefficient, $T_R/\left[\rho(\Omega R)^2\pi R^2\right]$
d_a	= Axial distance of point from axis of vortex ring/R
d_r	= Radial distance of point from plane of vortex ring/R
d_1	= Shortest distance from point to vortex ring/R
d_2	= Longest distance from point to vortex ring/R
$E(\tau)$	elliptic integral of second kind
h_h	height of hub above gimbal pivot point, cm
H	= Height of fuselage/R
H_R	rotor axial force, N
$K(\tau)$	elliptic integral of first kind
K_T	tip loss factor, Effective rotor radius/R
$\bar{n}$	normal vector
N	ellipse power or slipstream contraction factor
p	static pressure, Pa
p_t	total pressure, Pa
P	point designation (figs. 2 and 3)
q	dynamic pressure, $0.5\rho V_\infty^2$, Pa, or point designation (fig. 2)

r	= Radial polar coordinate/R or Wake radius/R or control point distribution (see fig. 2)
R	rotor radius or vortex-ring radius, m
R_C	= Root cutout/R
R_P	radial distance of point from axis of vortex ring, m
s	incremental surface
T	rotor thrust, N
V	velocity vector, m/sec
V_I	momentum induced velocity, m/sec
V_T	rotor tip speed, ΩR, m/sec
w	component of V, m/sec
W	= Width of fuselage/R
x,y,z	Cartesian coordinates in body axis
x_R,y_R,z_R	coordinates in TPP system
x_s,z_s	distance from moment reference center of gimbal pivot point, cm
Y_R	rotor side force
ZO	= Body camber/R
α	angle of attack, deg (see fig. 1(a))
β	angle of sideslip, deg
γ	rotor-shaft tilt angle, deg (see fig. 1(b))
Γ	vortex strength
λ	rotor inflow ratio, $(V_\infty \sin \alpha - V_I)/V_T$
μ	rotor advance ratio, $V_\infty \cos \alpha/V_T$
ρ	air density, kg/m^3
σ	source strength
τ	$= (d_2 - d_1)/(d_2 + d_1)$
ϕ	azimuthal polar coordinate, deg, or velocity potential

Φ total-velocity potential

χ wake skew angle measured from vertical axis, deg

ψ blade azimuth position, deg, or wake-area contraction ratio, A_∞/A_o (see fig. 1(b))

Ψ stream function

Ω rotor rotational speed, rad/sec (see fig. 1(b))

Subscripts:

f fuselage

i local condition

n normal

o at rotor disk

p perturbation due to fuselage

R rotor

s surface

t tangential

w wake

∞ free stream or fully contracted wake

Notation:

eff effective

HP hub plane

NFP no feathering plane

rpm revolutions per minute

TPP tip path plane

|| vector magnitude

Δ difference due to rotor wake

∇ gradient

$\bar{(\ )}$ vector

DISCUSSION OF THEORY

The numerical analysis method presented in this paper is based upon the panel method of reference 1 and an extension of the vortex-tube rotor-wake model derived from references 3 and 4.

Panel Method Theory

The panel method is derived from the conditions that the velocity potential Φ must satisfy Laplace's equation

$$\nabla^2\Phi = 0 \tag{1}$$

as well as two boundary conditions. The first boundary condition is the requirement of tangential flow at the impermeable body surface and can be written as

$$\left(\frac{\partial\Phi}{\partial\bar{n}}\right)_s = \bar{n} \cdot \nabla\Phi = 0 \tag{2}$$

The second boundary condition is that Φ must approach the nondisturbed free-stream potential at infinity. The velocity potential Φ is comprised of the free-stream potential ϕ_∞, a nonuniform onset or rotor-wake potential ϕ_w, and a disturbance potential due to the fuselage ϕ_p. Therefore Φ can be expressed as

$$\Phi = \phi_\infty + \phi_w + \phi_p \tag{3}$$

The gradient of the uniform onset potential is given in reference 1 as

$$\nabla\phi_\infty = -\bar{V}_\infty \tag{4}$$

and the gradient of the nonuniform onset potential is defined such that

$$\nabla\phi_w = -\Delta\bar{V}(P) \tag{5}$$

where $\Delta\bar{V}$ is dependent upon the position of point P. The disturbance potential is given as a source density distribution over the body surface such that

$$\phi_p(P) = \iint_s \frac{\sigma(q)}{r(P,q)}\,ds \tag{6}$$

where P is a point in space and q is a point on the surface which is a distance r from point P. (See fig. 2.) The function $\sigma(q)$ is the source density distribution.

Since equations (4) to (6) satisfy Laplace's equation and the infinity boundary condition, the source function σ can be calculated by using the boundary condition of tangential flow at the body surface (eq. (2)). For point P on the body surface, the normal derivative of equation (6) is shown in reference 13 to be

$$\frac{\partial \phi_p(P)}{\partial \bar{n}} = -2\pi\sigma(P) + \iint_S \frac{\partial}{\partial \bar{n}} \left[\frac{1}{r(P,q)}\right] \sigma(q)\, ds \tag{7}$$

The normal derivatives of ϕ_∞ and ϕ_w are

$$\frac{\partial \phi_\infty}{\partial \bar{n}} = -\bar{n} \cdot \bar{V}_\infty \tag{8}$$

and

$$\frac{\partial \phi_w}{\partial \bar{n}} = -\bar{n} \cdot \Delta\bar{V}(P) \tag{9}$$

respectively. Thus, combining equations (7), (8), and (9) gives

$$2\pi\sigma(P) - \iint_S \frac{\partial}{\partial \bar{n}} \left[\frac{1}{r(P,q)}\right] \sigma(q)\, ds = -\bar{n} \cdot \left[\bar{V}_\infty + \Delta\bar{V}(P)\right] \tag{10}$$

where the right side of equation (10) is the normal onset velocity (uniform plus nonuniform) and the left side of the equation is the normal perturbation velocity.

In panel methods equation (10) is typically solved by approximating a body surface with discrete quadrilateral panels. Thus, equation (10) can be expressed as a matrix equation of the form

$$\sum_{j=1}^{N} \left(\bar{n}_i \cdot \bar{V}_{ij}\right)\sigma_j = -\bar{n}_i \cdot \left(\bar{V}_\infty + \Delta\bar{V}\right)_i \qquad (i = 1, 2, 3, \ldots, N) \tag{11}$$

where N is the total number of panels and $\bar{V}_{ij}$ is a matrix of aerodynamic influence coefficients which is a function of geometry only. (See ref. 13 for details.) Therefore equation (10) has been replaced by a set of linear

algebraic equations. This system of equations is solved by standard numerical matrix techniques to obtain the source strengths σ_j.

The velocity vector at each panel control point is obtained by using the source strengths and aerodynamic influence coefficients. These final velocities are given by

$$\bar{V}_i = \sum_{j=1}^{N} \bar{V}_{ij}\sigma_j + \bar{V}_\infty + \Delta\bar{V}_i \qquad (i = 1, 2, \ldots, N) \qquad (12)$$

The panel pressure coefficient $C_{p,i}$ is defined as

$$C_{p,i} = \frac{p_i - p_\infty}{q_\infty} \qquad (13)$$

Since the static pressure p_i at the panel center can be expressed as the difference between the total and the dynamic pressure at panel i

$$C_{p,i} = \frac{p_{t,i} - q_i - p_\infty}{q_\infty} \qquad (14)$$

Also, the total pressure $p_{t,i}$ can be expressed as the sum of the uniform onset flow total pressure $p_{t,\infty}$ plus a local total-pressure variation $\Delta p_{t,i}$ due to the rotor wake. Therefore

$$C_{p,i} = \frac{p_{t,\infty} - q_i - p_\infty + \Delta p_{t,i}}{q_\infty} \qquad (15a)$$

or since $p_{t,\infty} = q_\infty + p_\infty$,

$$C_{p,i} = \frac{q_\infty + p_\infty - q_i - p_\infty + \Delta p_{t,i}}{q_\infty} \qquad (15b)$$

The free-stream static pressure p_∞ is eliminated, thus giving

$$C_{p,i} = \frac{q_\infty - q_i + \Delta p_{t,i}}{q_\infty} \qquad (15c)$$

and by replacing q_∞ with $0.5\rho V_\infty^2$ gives

$$C_{p,i} = \frac{(0.5)\rho|\bar{V}_\infty|^2 - (0.5)\rho|\bar{V}_i|^2}{(0.5)\rho|\bar{V}_\infty|^2} + \frac{\Delta p_{t,i}}{q_\infty} \tag{15d}$$

which reduces to

$$C_{p,i} = 1 - \frac{|\bar{V}_i|^2}{|\bar{V}_\infty|^2} + \frac{\Delta p_{t,i}}{q_\infty} \tag{15e}$$

The term $\Delta p_{t,i}$ will be discussed in the section concerned with the rotor-wake modeling. Body forces and moments are calculated by summing the pressures over the surface of the body.

Vortex-Tube Theory

The effect of the rotor flow field is added to the panel method solution of the body aerodynamics as an onset flow disturbance $\Delta\bar{V}_i$ (eqs. (11) and (12)) and as a total-pressure variation $\Delta p_{t,i}/q_\infty$ (eq. (15e)) at each panel control point. The onset flow disturbance is determined from the vortex-tube method, and the total-pressure variation is determined from momentum theory.

The vortex-tube method of wake representation which was used is a variation of the method described in references 3 and 4. In the vortex-tube method, the wake is defined by a series of concentric vortex tubes each of which consists of a finite but large number of vortex rings. (See fig. 3.)

The stream function at a point relative to a vortex ring is shown in reference 14 to be

$$\Psi(P) = \frac{\Gamma R}{2\pi}(d_1 + d_2)\left[K(\tau) - E(\tau)1\right] \tag{16}$$

where Γ is the strength of the vortex ring, R is its radius, d_1 and d_2 are the minimum and maximum distances, respectively, from point P to the ring (see fig. 3), and $K(\tau)$ and $E(\tau)$ are complete elliptic integrals of the first and second kinds, respectively. The parameter τ is defined as

$$\tau = \frac{d_2 - d_1}{d_2 + d_1} \tag{17}$$

The axial component of velocity of the stream function Ψ is

$$V_n = -\frac{1}{R_P}\frac{d\Psi}{dR_P} \tag{18}$$

where R_P is the radial distance of point P from the vortex-ring axis. In reference 6, equation (18) is expressed as

$$V_n = \frac{\Gamma}{2\pi R_P}(AB + CDF) \tag{19}$$

where

$$A = K(\tau) - E(\tau) \tag{20}$$

$$B = \frac{d_r - 1}{d_1} + \frac{d_r + 1}{d_2} \tag{21}$$

$$C = d_1 + d_2 \tag{22}$$

$$D = \frac{\tau E(\tau)}{1 - \tau^2} \tag{23}$$

$$F = 1 - \frac{1 + {d_r}^2 + {d_a}^2 - d_1 d_2}{2{d_r}^2} - \frac{(1 + d_r){d_1}^2 - (1 - d_r){d_2}^2}{2d_r d_1 d_2} \tag{24}$$

$$d_1 = \left[{d_a}^2 + (d_r - 1)^2\right]^{1/2} \tag{25}$$

$$d_2 = \left[{d_a}^2 + (d_r + 1)^2\right]^{1/2} \tag{26}$$

where d_a is the nondimensional axial distance from the plane of the ring to point P and d_r is the nondimensional radial distance from the axis of the ring to point P.

The axial component of velocity for a vortex tube can be expressed as

$$V_n = \sum_{j=1}^{K} \frac{\Gamma}{2\pi R_{P,j}} \left(A_j B_j + C_j D_j F_j\right) \tag{27}$$

where K is the total number of vortex rings. The vortex-ring circulation Γ is obtained by requiring that V_n be equal to the average induced velocity at the center of the rotor disk with uniform loading.

Reference 4 shows that nonuniform disk loading can be represented by a series of concentric vortex tubes. Loading is either added (positive vorticity) or subtracted (negative vorticity) from the tip vortex-tube strength to vary the loading across the rotor disk.

In the present method, wake contraction was added by varying the vortex-ring radii according to empirical relationships given in reference 15. The ratio of the radius of the final contracted wake to the rotor radius is expressed as

$$\frac{r_\infty}{r_o} = 0.707 + 0.1418\left(1.0 - e^{-C_T \cdot 58.77}\right) \tag{28}$$

or in terms of area

$$\psi = \frac{A_\infty}{A_o} = \left(\frac{r_\infty}{r_o}\right)^2 \tag{29}$$

The area ratio at a given axial location z_R is expressed as

$$\frac{A_i}{A_o} = \psi + (1.0 - \psi)e^{z_R \cdot N} \tag{30}$$

where N is a slipstream contraction factor based on experimental data given in reference 15.

Swirl is introduced as a tangential component of induced velocity since the lift vector of a blade element is in reality not perpendicular to the disk plane but is perpendicular to the local resultant velocity (ref. 15). Therefore, the local tangential velocity V_t can be calculated by the equation

$$V_t = \frac{1}{\Omega R} \frac{V_I^2}{\left(\frac{A_i}{A_o}\right)^2} \tag{31}$$

where V_I is the average induced downwash at the rotor disk calculated from momentum theory.

The pressure coefficient used in the panel method was given as equation (15e) which includes a total-pressure term. The derivation of the total-pressure term is given in the appendix and is expressed as

$$\frac{\Delta p_{t,i}}{q_\infty} = \frac{\left|\bar{V}_\infty + \Delta\bar{V}\right|^2}{\left|\bar{V}_\infty\right|^2} - 1.0 + \frac{1.5C_T}{\mu^2}\left(\frac{\frac{A_i}{A_o} - \frac{A_\infty}{A_o}}{1 - \frac{A_\infty}{A_o}}\right) \tag{32}$$

Equation (32) is evaluated at each panel control point.

COMPUTER CODE DESCRIPTION

Analytical results were obtained by using the panel method of reference 1 coupled with the vortex-tube method as previously discussed. In the computer code architecture, the wake calculation program was added as a subprogram to the panel method program. The wake program is called after all the body geometry has been input and the control points (panel centroids) have been calculated. The vortex program then calculates rotor-induced velocities and total-pressure variations at the panel control points and returns these values to the main program. Source distributions are calculated based upon the total onset flow, and velocity distributions are calculated based upon these source distributions and the onset flow. The pressure distributions are then calculated based upon the velocity distribution and the differential total pressure as calculated in the vortex-tube program.

Modifications to the Panel Method Program

Modifications to the panel method program included the addition of arrays to store the nonuniform onset flows and total-pressure values, addition of the nonuniform onset flow term to equations (11) and (12), and the addition of the total-pressure variation term to equation (15e).

Vortex-Tube Program

The vortex-tube program requires as input: (1) Coordinates of panel centers; (2) rotor geometry including hub position, tip-path-plane angle of attack, fuselage angle of attack, disk radius, and root cutout; and (3) performance parameters including C_T, V_T, tip loss factor, and radial blade loading.

Initial calculations determine general rotor-wake parameters which define the wake geometry. These parameters include the average induced velocity, the contraction ratio, the wake skew angle, and the static-pressure differential at the rotor disk.

The average induced velocity is calculated by using the momentum theory. For hover

$$V_I = V_T\left(0.5 \cdot C_T \cdot A_{eff}\right)^{1/2} \tag{33}$$

where $A_{eff} = 1.0/\left(K_T^2 - R_c^2\right)$ is a correction for the effective rotor area, K_T is a tip loss factor, and R_c is the root cutout.

For forward flight

$$V_I = 0.5 \cdot V_T \cdot C_T \cdot A_{eff}/\left(\mu^2 + \lambda^2\right)^{1/2} \tag{34}$$

which is solved in an iterative fashion since λ is a function of V_I. Equation (33) is used as an initial estimate of V_I to calculate the inflow ratio λ. The inflow ratio and induced velocity are alternately calculated until V_I converges to a solution.

Initial observations of the skew angle measured from the wind-tunnel test (which is discussed later) indicated that the skew angle is well approximated by the expression

$$\chi = \tan^{-1}\left(\frac{-\mu}{\psi\lambda}\right) \tag{35}$$

where ψ is the contraction ratio and is calculated by using equation (29).

The following calculations are repeated for each panel control point. After the coordinates of the control point are rotated and translated to the rotor tip-path-plane (TPP) coordinate system, the axial induced velocity is calculated by using 1 to 15 concentric vortex tubes (depending upon the radial variation of disk loading). Each tube consists of 101 discrete vortex rings, the radii of which vary with the expression

$$\frac{r_i}{r_o} = \left[\psi + (1.0 - \psi)e^{z_R N}\right]^{1/2} \tag{36}$$

where z_R is the axial distance of the ring beneath the rotor and N is the empirical slipstream contraction factor. Therefore, the total axial induced velocity at one control point is the sum of the contributions of 101 vortex rings times the number of vortex tubes.

After the induced axial velocity is obtained, the tangential velocity (swirl) is calculated by using equation (31). The axial and tangential velocities are then rotated into the fuselage Cartesian axis system. The local

total-pressure variation is calculated by using equation (32). These rotor-induced velocities and total-pressure values are then returned to the panel method program. These rotor computations add approximately 5 percent to the running time of the panel method program.

EXPERIMENTAL DATA

Validation of new analytical methods generally requires experimental data as a basis for comparison. Although reference 16 presents surface pressures of three helicopter models with a 1-meter-diameter, two-bladed rotor, the pressure orifice locations were considered too sparse to allow for accurate comparisons with the analytical method. Therefore a wind-tunnel investigation using a helicopter model with more closely spaced pressure orifices was conducted in the Langley V/STOL Tunnel. A photograph of the model in the test section is presented as figure 4.

Model Description

The rotor system used in this investigation consisted of a 3.15-meter-diameter, four-bladed rotor. The hub was fully articulated with flapping and lagging hinges coincident at 4.8-percent radius. The rotor blades had -8° twist, an untapered planform, and square tips. Details of the rotor system may be found in table I.

The fuselage shape for this test is mathematically defined. At a given fuselage station x, the cross-section y- and z-coordinates are defined by the local fuselage height H, width W, camber line ZO, and elliptical power N as follows.

The parameters H, W, ZO, and N are obtained by applying the function

$$f(x) = C_6 + C_7\left[C_1 + C_2\left(\frac{x + C_3}{C_4}\right)^{C_5}\right]^{1/C_8} \tag{37}$$

with separate sets of constants C_1 to C_8 for each of the four cross-section parameters H, W, ZO, and N. As shown in figure 5, the fuselage is divided into four regions and the pylon into two regions with a set of constants for each region. These constants are given in table II.

By using the three parameters H, W, and N as obtained from equation (37), the cross section can be defined by the polar coordinates r and ϕ such that for a given ϕ

$$r(\phi) = \left[\frac{(0.5H + 0.5W)^N}{(0.5H \sin)^N + (0.5W \cos)^N}\right]^{1/2} \tag{38}$$

The body Cartesian coordinates are then obtained from the relationships

$$y = r(\phi) \sin \phi \tag{39}$$

$$z = r(\phi) \cos \phi + ZO \tag{40}$$

Test Conditions

The experimental data presented in this paper were obtained for an advance ratio of 0.05 at the test conditions as given in table III. The wind-tunnel test section, which measures 4.42 meters by 6.63 meters, was configured with the walls and ceiling removed. Angle of attack and test-section dynamic pressure were corrected for wall effects by using methods described in reference 17. All tests were conducted with the moment reference center of the model on the center line of the test section. This position corresponds to a rotor height of 1.84 times the rotor radius. The pressure data were averaged for 50 samples over 5 seconds of sampling time. The data used in this paper were obtained from reference 18.

PRESENTATION OF RESULTS

The results obtained from the computer code and the experimental tests are presented in the following figures:

	Figure
Isolated rotor-induced velocities in $y = 0$ plane for $\mu = 0.05$ . . .	6
Calculated x- and z-components of total velocity on left side of fuselage for $\mu = 0.05$	7
Pressure distribution along top center line of fuselage for $\mu = 0.05$	8
Lateral pressure distributions at four fuselage stations for $\mu = 0.05$	9
Separation and swirl effects on fuselage cross-section pressure distribution	10

DISCUSSION OF RESULTS

Results obtained from the analytical method are presented in the form of rotor-wake onset velocity distributions, total-surface velocity distributions, and surface pressure distributions. These three outputs are useful in analyzing the aerodynamics of a helicopter in different ways.

Figure 6 presents the induced velocity vectors of the isolated rotor in a vertical plane along the center line of the hub (i.e., $y_R = 0$) at four thrust levels. Evident in this figure is the contraction and skew angle of the rotor wake as calculated by the rotor-wake segment of the program. As would be expected, the skew angle decreases with increasing thrust as the momentum

inflow velocity increases. The skew angle ranges from approximately 40° at the low thrust to 25° at the high thrust. Full wake contraction occurs at approximately 50-percent radius below the rotor disk.

The inflow variation at the rotor disk is also evident with zero inflow at the center and maximum downwash at approximately 80-percent radius. There is also a substantial difference in inflow levels for the front and aft portions of the rotor. These variations decreased downstream of the rotor.

In figure 7 the x- and z-components of the total-velocity vectors on the left side of the fuselage are plotted. These results are obtained from the panel method as rotor-wake effects on the fuselage. Wake boundaries are discernible on the nose and tail cone as large gradients in the vertical component of the total velocity. These total velocities follow the same general pattern of the isolated rotor-induced velocities. Longitudinal variations of vertical velocity are particularly evident on the tail cone. The effect of the root cutout is seen as a stagnation region below and slightly behind the hub location at 35-percent-body length.

Figures 8 and 9 present comparisons of surface-pressure coefficients for experimental data and results obtained from the analytical method. Although the pressure distribution on the entire fuselage surface is not shown, these figures illustrate the character of the longitudinal and lateral pressure distributions.

In figure 8 the pressure coefficients and geometry of the top center line of the fuselage are given. Since the top center line would be considered the stagnation line for a rotor downwash, the large positive values of C_p should be proportional to the square of the downwash velocity. Very evident in this figure is the nonuniformity of the longitudinal downwash distribution as is seen in the velocity vectors of figures 6 and 7.

Even though the overall character of the experimental and analytical distributions match, several discrepancies are evident. For the low-thrust case (fig. 8(a)), the wake impingement location (point of maximum C_p) is not coincident ($x/R \approx 0.25$) because the analytical model assumes a constant skew angle and the actual wake is curved.

Other discrepancies in figure 8(a) include the overall levels of the downwash with the analytical method underpredicting the pressure coefficients and the seemingly higher experimental downwash from the front part of the rotor disk as compared with the aft portion. These discrepancies are not evident at the three higher thrust levels, although the analytical method does slightly underpredict the pressures on the aft portion of the fuselage. This underprediction may at least be partly due to the probable separation of the rotor pylon which is not modeled in the analytical method.

Experimentally, the forward location of impingement varied from $x/R = 0.25$ for $C_T = 0.0033$ to $x/R = 0.15$ for $C_T = 0.0082$, which corresponds to skew angles of approximately 40° to 25°, respectively. The aft impingement point

cannot be discerned from the experimental data as it occurs slightly aft of the last pressure orifices.

Figure 9 gives the pressure distribution, experimental orifice location, and panel centroid locations at four fuselage stations and four thrust levels. These four stations are $x/R = 0.20$, 0.30, 1.34, and 1.53. Two are ahead of the rotor hub and two are behind. The experimental data, especially at the higher values of C_T, in these figures generally follow an M-pattern with large negative values of C_p where the downwash accelerates around the cross-section corners and large positive values of C_p at the top (z/R maximum) and bottom (z/R minimum) stagnation points. The analytical data have this same M-character but quantitatively differ at two regions. The analytical method seems to underpredict the flow acceleration around the top corner (z/R positive) and to overpredict the stagnation pressure on the bottom side. The reason for the first discrepancy may be the coarseness of the paneling at the corners and the fact that the wake program generally underpredicts the downwash levels. The second discrepancy is attributed to flow separating at the lower corner of the cross section as illustrated in figure 10. As mentioned previously, a separation model was not included in this panel method program.

Also evident in figures 9 and 10 is the effect of swirl. A crossflow on a fuselage section would decrease the flow acceleration at the corners on one side and increase the acceleration on the opposite side; for example, $C_T = 0.0082$. At $x/R = 0.20$ (see fig. 9(m)), the difference in the experimental pressures at the top corner for the right and left side is 4.75 with the left side being higher (more negative C_p). The analytical results again underpredict these corner pressures. Behind the rotor at $x/R = 1.53$ (fig. 9(p)), the pressure orifice spacing was not fine enough to indicate the quantitative difference of the right and left side, but the right-side pressure distribution indicates a higher acceleration. Therefore the crossflow right to left forward of the hub and left to right aft of the hub indicates a definite swirl in the direction of rotor rotation as modeled by the wake program.

CONCLUSIONS

The surface pressure and velocity distributions about a helicopter fuselage immersed in a rotor wake have been calculated by using a potential-flow panel method having a vortex-tube rotor model. The pressure distributions have been compared with experimental results obtained from a 3.14-meter-diameter rotor wind-tunnel model with a general helicopter fuselage. The conclusions are summarized as follows:

1. The measured and predicted pressure on the fuselage at low rotor-wake skew angles varies significantly both longitudinally and laterally as a result of the influence of the rotor wake.

2. The panel-method—vortex-tube combination, which accounts for skew angle, contraction, and total-pressure variations, can adequately calculate the character of the time-averaged pressure and velocity distributions if the tube

geometry (skew angle and contraction) is modeled correctly, the total-pressure corrections are accounted for, and the swirl velocities are added.

3. Increased accuracy would be obtained with the inclusion of a flow-separation technique and a curved rotor-wake model.

Langley Research Center
National Aeronautics and Space Administration
Hampton, VA 23665
April 17, 1980

APPENDIX

CALCULATION OF TOTAL PRESSURE IN THE ROTOR WAKE

Momentum theory in hover considers the rotor as a disk as shown in the following sketch:

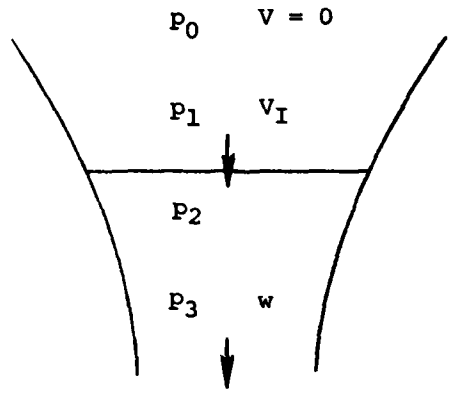

Location 0 is at infinity; location 1 is immediately before the disk; location 2 is immediately following the disk; and location 3 is at the point of full contraction. The average induced velocity through the disk is V_I, and the fully contracted wake velocity is w. The static pressures are p_0, p_1, p_2, and p_3 at locations 0, 1, 2, and 3, respectively.

Bernoulli's equation for steady, inviscid, incompressible flow with negligible gravitational force and no work done is

$$p_t = p + 0.5\rho V^2 \tag{A1}$$

where p_t is the total pressure, p is the static pressure, ρ is the density, and V is the local velocity. Applying equation (A1) to the four locations and assuming that $p_{t,0} = p_{t,1}$ and $p_{t,2} = p_{t,3}$ gives

$$p_0 = p_1 + 0.5\rho V_I^2 \tag{A2}$$

and

$$p_3 + 0.5\rho w^2 = p_2 + 0.5\rho V_I^2 \tag{A3}$$

The thrust on the disk can be expressed as

$$T = (p_2 - p_1)A \tag{A4}$$

where A is the disk area.

Subtracting equation (A2) from equation (A3) and solving for $(p_2 - p_1)$ gives

$$p_2 - p_1 = p_3 - p_0 + 0.5\rho w^2 \tag{A5}$$

However $p_3 - p_0 = 0$, if the assumption is made that the static pressure in the fully contracted wake is equal to the ambient static pressure. By making this assumption and combining equations (A4) and (A5), the rotor thrust is expressed as

$$T = 0.5\rho w^2 A \tag{A6}$$

From momentum theory

$$T = \rho A V_I w \tag{A7}$$

Equating equations (A6) and (A7) and solving for w gives

$$w = 2.0 V_I \tag{A8}$$

Using equation (A8) in equation (A5) gives

$$p_2 - p_1 = 2.0\rho V_I^2 \tag{A9}$$

From equation (A3), assuming that $p_3 = p_0$

$$p_2 - p_0 = 0.5\rho w^2 - 0.5\rho V_I^2 \tag{A10}$$

Again, by substituting $w = 2.0V_I$, equation (A10) becomes

$$p_2 - p_0 = 1.5\rho V_I^2 \tag{A11}$$

or

$$p_2 - p_0 = 0.75(p_2 - p_1) \tag{A12}$$

Therefore the static-pressure rise immediately behind the disk is three-fourths of the static-pressure rise across the disk. By applying the definition

$$C_T = \frac{T}{\rho A V_T^2} \tag{A13}$$

to equation (A4), $p_2 - p_1$ becomes

$$p_2 - p_1 = C_T \rho V_T^2 \tag{A14}$$

Substituting equation (A14) into equation (A12) gives

$$p_2 - p_0 = 0.75 C_T \rho V_T^2 \tag{A15}$$

or by nondimensionalizing by $0.5\rho V_\infty^2$ and making the approximation $\mu = V_\infty/V_T$, equation (A15) becomes

$$\frac{p_2 - p_0}{0.5\rho V_\infty^2} = \frac{1.5C_T}{\mu^2} \tag{A16}$$

which expresses the difference in static pressure across the wake boundary.

The difference in total pressure inside the rotor wake at a point i and free stream can be expressed as

$$\frac{\Delta p_{t,1}}{q_\infty} = \frac{\Delta p_i}{q_\infty} + \frac{\Delta q_i}{q_\infty} \tag{A17}$$

By assuming that the static-pressure variation at point 2 in forward flight is the same as hover and that the static-pressure variation goes to zero for the fully contracted wake, p can be expressed as

$$\frac{\Delta p_i}{q_\infty} = \frac{1.5C_T}{\mu^2}\left(\frac{\frac{A_i}{A_o} - \frac{A_\infty}{A_o}}{1 - \frac{A_\infty}{A_o}}\right) \tag{A18}$$

where A_i is the wake cross-section area at point i.

The difference in dynamic pressure can be expressed as

$$\frac{\Delta q_i}{q_\infty} = \frac{|\bar{V}_\infty + \Delta\bar{V}_i|^2}{|\bar{V}_\infty|^2} - 1.0 \tag{A19}$$

where $\Delta\bar{V}_i$ is the resultant of the axial and tangential wake velocities. Therefore

$$\frac{\Delta p_{t,i}}{q_\infty} = \frac{|\bar{V}_\infty + \Delta\bar{V}_i|^2}{|\bar{V}_\infty|^2} - 1.0 + \frac{1.5C_T}{\mu^2}\left(\frac{\frac{A_i}{A_o} - \frac{A_\infty}{A_o}}{1 - \frac{A_\infty}{A_o}}\right) \tag{A20}$$

REFERENCES

1. Hess, John L.: The Problem of Three-Dimensional Lifting Potential Flow and Its Solution by Means of Surface Singularity Distribution. Comput. Methods Appl. Mech. & Eng., vol. 4, no. 3, Nov. 1974, pp. 283-319.

2. Coleman, Robert P.; Feingold, Arnold M.; and Stempin, Carl W.: Evaluation of the Induced-Velocity Field of an Idealized Helicopter Rotor. NACA WR L-126, 1945. (Formerly NACA ARR L5E10.)

3. Castles, Walter, Jr.; and De Leeuw, Jacob Henri: The Normal Component of the Induced Velocity in the Vicinity of a Lifting Rotor and Some Examples of Its Application. NACA Rep. 1184, 1954. (Supersedes NACA TN 2912.)

4. Heyson, Harry H.; and Katzoff, S.: Induced Velocities Near a Lifting Rotor With Nonuniform Disk Loading. NACA Rep. 1319, 1957. (Supersedes NACA TN 3690 by Heyson and Katzoff and TN 3691 by Heyson.)

5. Heyson, Harry H.: Equations for the Induced Velocities Near a Lifting Rotor With Nonuniform Azimuthwise Vorticity Distribution. NASA TN D-394, 1960.

6. Goldstein, Sydney: On the Vortex Theory of Screw Propellers. Proc. R. Soc. (London), ser. A, vol. 123, no. 792, Apr. 6, 1929, pp. 440-465.

7. Castles, Walter, Jr.; and Durham, Howard L., Jr.: The Computed Instantaneous Velocities Induced at the Blade Axes by the Skewed Helical Vortices in the Wake of a Lifting Rotor in Forward Flight. Contract No. Nonr 991(05), Georgia Inst. Technol., Mar. 1959. (Available from DTIC as AD 210 613.)

8. Brady, W. G.; and Crimi, P.: Representation of Propeller Wakes by Systems of Finite Core Vortices. CAL-BB-1665-S-2 (Contract No. NONR-3691-00), Cornell Aeronaut. Lab., Inc., Feb. 1965. (Available from DTIC as AD 612 007.)

9. Theodorsen, Theodore: Theory of Static Propellers and Helicopter Rotors. [Preprint] No. 326, 25th Annual National Forum Proceedings, American Helicopter Soc., Inc., May 1969.

10. Clark, David R.; and Leiper, Albert C.: The Free Wake Analysis - A Method for the Prediction of Helicopter Rotor Hovering Performance. [Preprint] No. 321, 25th Annual National Forum Proceedings, American Helicopter Soc., Inc., May 1969.

11. Sadler, S. G.: A Method for Predicting Helicopter Wake Geometry, Wake-Induced Flow and Wake Effects on Blade Airloads. Preprint No. 523, 27th Annual National V/STOL Forum, American Helicopter Soc., May 1971.

12. Landgrebe, Anton J.: An Analytical and Experimental Investigation of Helicopter Rotor Hover Performance and Wake Geometry Characteristics. USAAMRDL Tech. Rep. 71-24, U.S. Army, June 1971. (Available from DTIC as AD 728 835.)

13. Kellogg, Oliver Dimon: Foundations of Potential Theory. Frederick Ungar Pub. Co., 1929.

14. Glauert, H.: On the Contraction of the Slipstream of an Airscrew. R. & M. No. 1067, British A.R.C., 1926.

15. Stepniewski, W. Z.: Rotary-Wing Aerodynamics. Volume I - Basic Theories of Rotor Aerodynamics (With Application to Helicopters). NASA CR-3082, 1979.

16. Wilson, John C.; and Mineck, Raymond E.: Wind-Tunnel Investigation of Helicopter-Rotor Wake Effects on Three Helicopter Fuselage Models. NASA TM X-3185, 1975.

17. Heyson, Harry H.: Use of Superposition in Digital Computers To Obtain Wind-Tunnel Interference Factors for Arbitrary Configurations, With Particular Reference to V/STOL Models. NASA TR R-302, 1969.

18. Freeman, Carl E.; and Mineck, Raymond E.: Fuselage Surface Pressure Measurements of a Helicopter Wind-Tunnel Model With a 3.15-Meter Diameter Single Rotor. NASA TM-80051, 1979.

TABLE I.- MODEL GEOMETRY

Fuselage:	
Moment reference center:	
x	0.690R
y	0R
z	0R
Length	2.0R
Rotor:	
Hub coordinates:	
x	0.690R
y	0R
z	0.274R
Number of blades	4
γ, deg	2
x_s	0.009R
z_s	0.034R
h_h	0.090R
Root cutout	0.20R
Chord, m	0.108
Radius, R, m	1.574
Twist, deg	-8.0
Flapping inertia, kg-m^2	0.653
Solidity	0.0871
Airfoil section	NASA RC-10-(B) M002

TABLE II.- PARAMETERS

Function	x/R	C_1	C_2	C_3	C_4	C_5	C_6	C_7	C_8
				Fuselage					
H	0 → 0.4	1.0	-1.0	-0.4	0.4	1.8	0	0.25	1.8
W	↓	1.0	-1.0	-.4	.4	2.0	0	.25	2.0
Z0		1.0	-1.0	-.4	.4	1.8	-.08	.08	1.8
N		2.0	3.0	0	.4	1.0	0	1.0	1.0
H	0.4 → 0.8	.25	0	0	0	0	0	1.0	1.0
W	↓	.25	0	0	0	0	0	1.0	1.0
Z0		8.0	0	0	0	0	0	1.0	1.0
N		5.0	0	0	0	0	0	1.0	1.0
H	0.8 → 1.9	1.0	-1.0	-.8	1.1	1.5	.05	.2	.6
W	↓	1.0	-1.0	-.8	1.1	1.5	.05	.2	.6
Z0		1.0	-1.0	-.8	1.1	1.5	.04	-.04	.6
N		5.0	-3.0	-.8	1.1	1.0	0	1.0	1.0
H	1.9 → 2.0	1.0	-1.0	-1.9	.1	2.0	0	.05	2.0
W	↓	1.0	-1.0	-1.9	.1	2.0	0	.05	2.0
Z0		.04	0	0	0	0	0	1.0	1.0
N		2.0	0	0	0	0	0	1.0	1.0
				Pylon					
H	0.4 → 0.8	1.0	-1.0	-0.8	0.4	3.0	0	0.2	3.0
W	↓	1.0	-1.0	-.8	.4	3.0	0	.172	3.0
Z0		.122	0	0	0	0	0	1.0	1.0
N		5.0	0	0	0	0	0	1.0	1.0
H	0.8 → 1.018	1.0	-1.0	-.8	.218	2.0	0	.2	2.0
W	↓	1.0	-1.0	-.8	.218	2.0	0	.172	2.0
Z0		1.0	-1.0	-.8	1.1	1.5	.065	.06	.6
N		.122	0	0	0	0	0	1.0	1.0

TABLE III.- TEST CONDITIONS

Run	Point	μ	α_f	β_f	Rotor speed, rpm	C_T	a_{1s}	b_{1s}
20	169	0.050	1.23	0	1200	0.00340	-1.07	0.06
20	170	.050	0	0	1200	.00502	-.92	.12
20	171	.050	0	0	1200	.00659	-.81	.07
20	172	.050	0	0	1200	.00816	-.69	.15

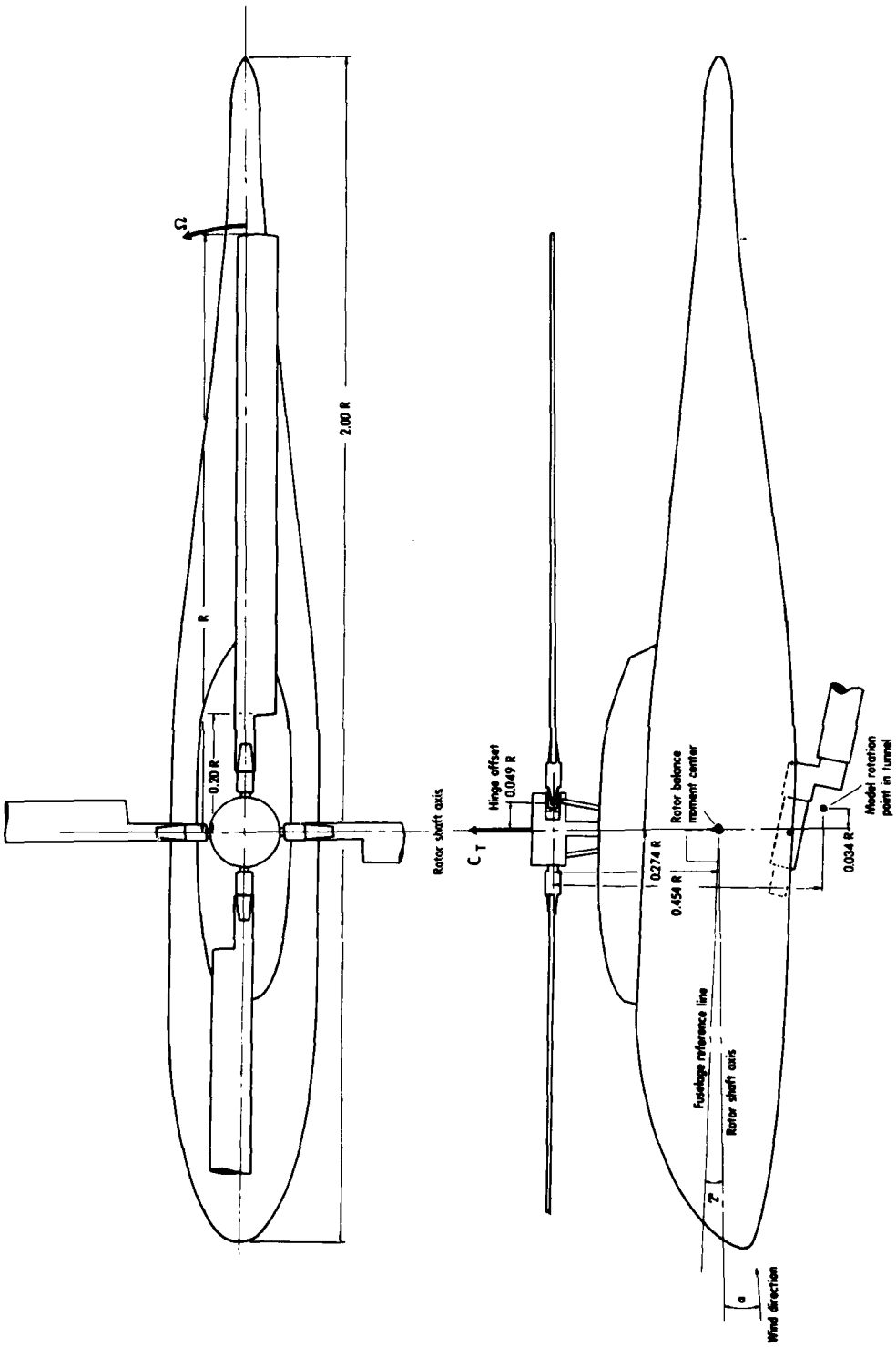

(a) Fuselage.

Figure 1.- Axes and sign conventions.

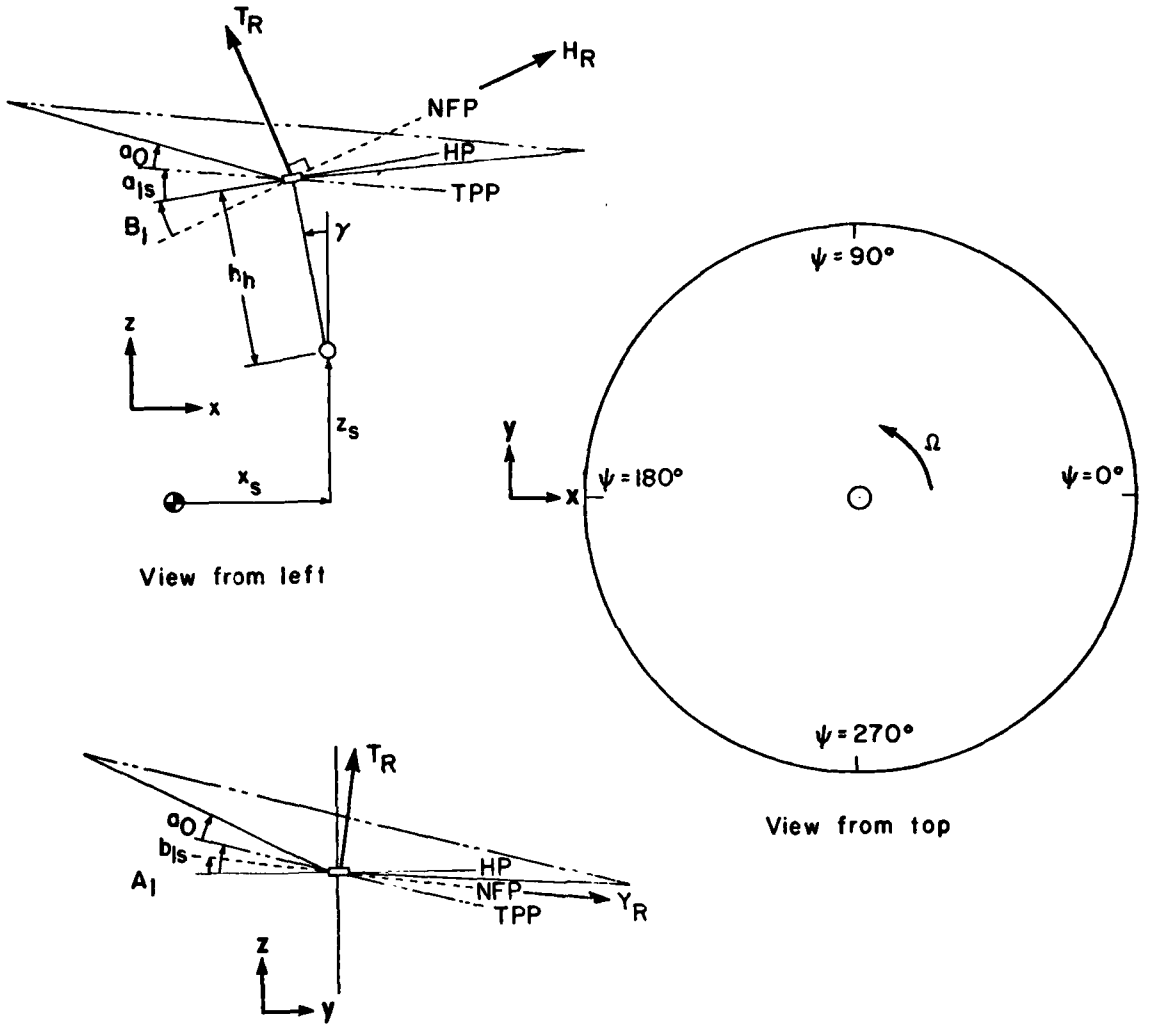

(b) Rotor system.

Figure 1.- Concluded.

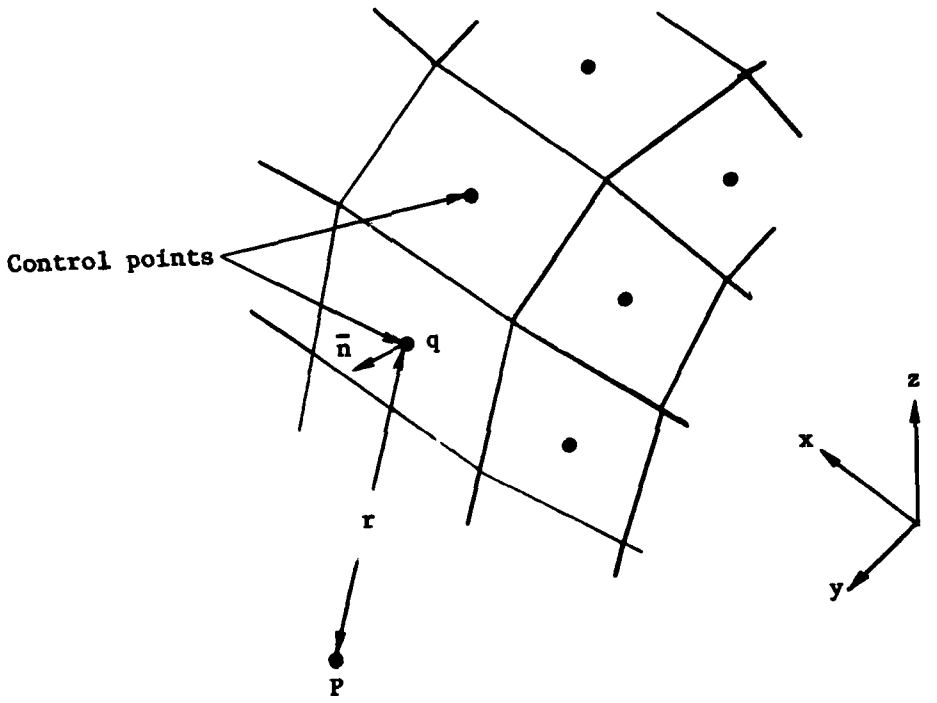

Figure 2.- Panel method influence parameters.

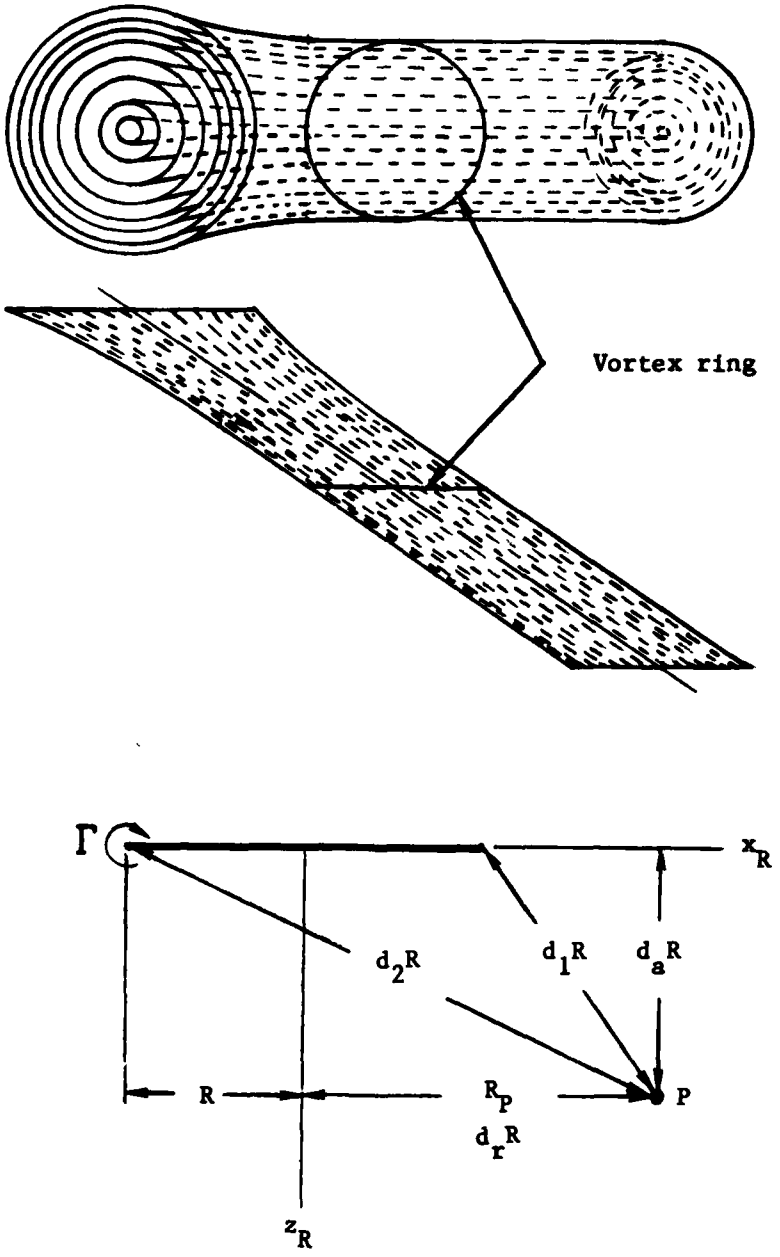

Figure 3.- Vortex-ring parameters.

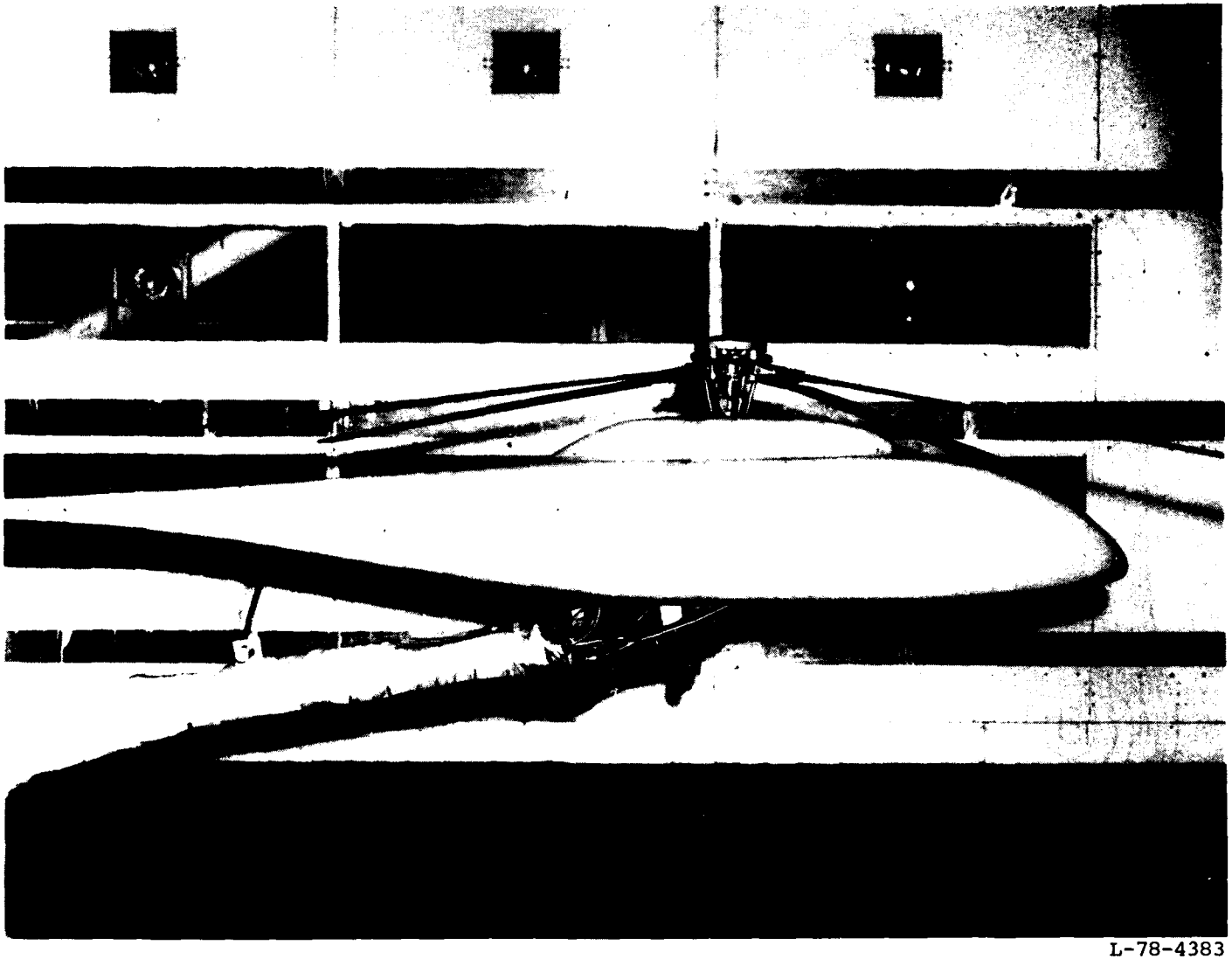

L-78-4383

Figure 4.- Wind-tunnel model installed in test section of Langley V/STOL Tunnel.

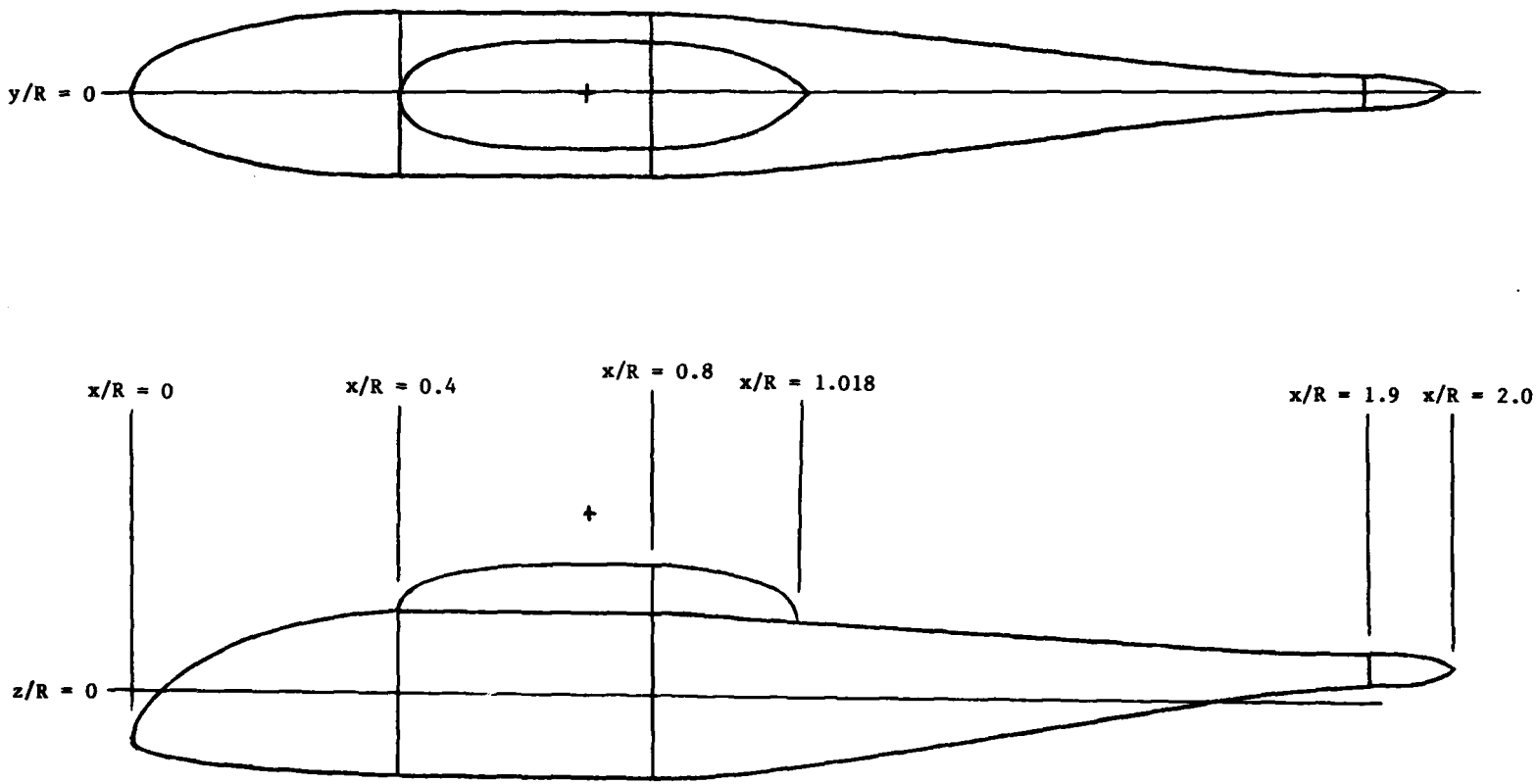

Figure 5.- Fuselage component regions.

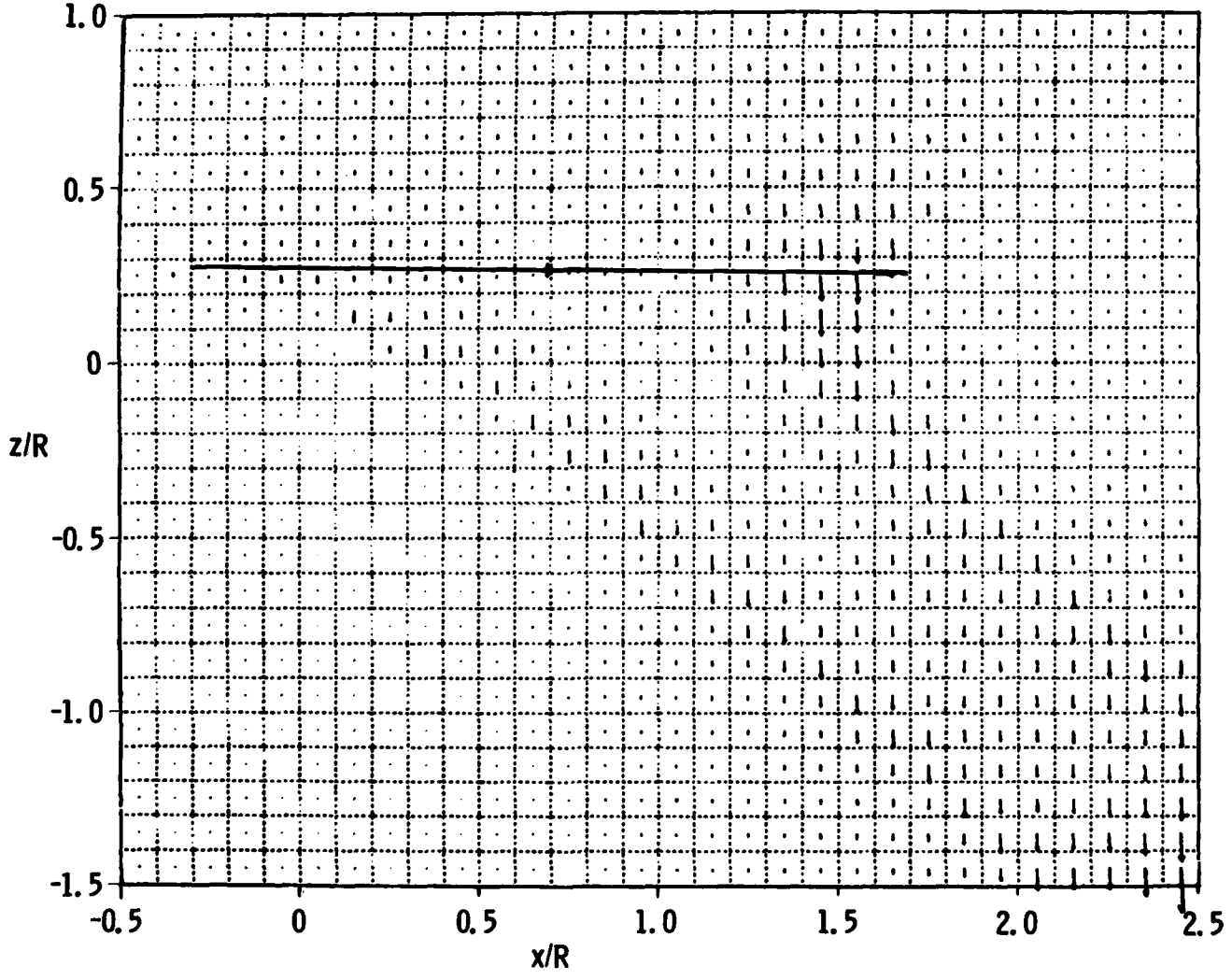

(a) $C_T = 0.0034$.

Figure 6.- Isolated rotor-induced velocities in $y = 0$ plane for $\mu = 0.05$.

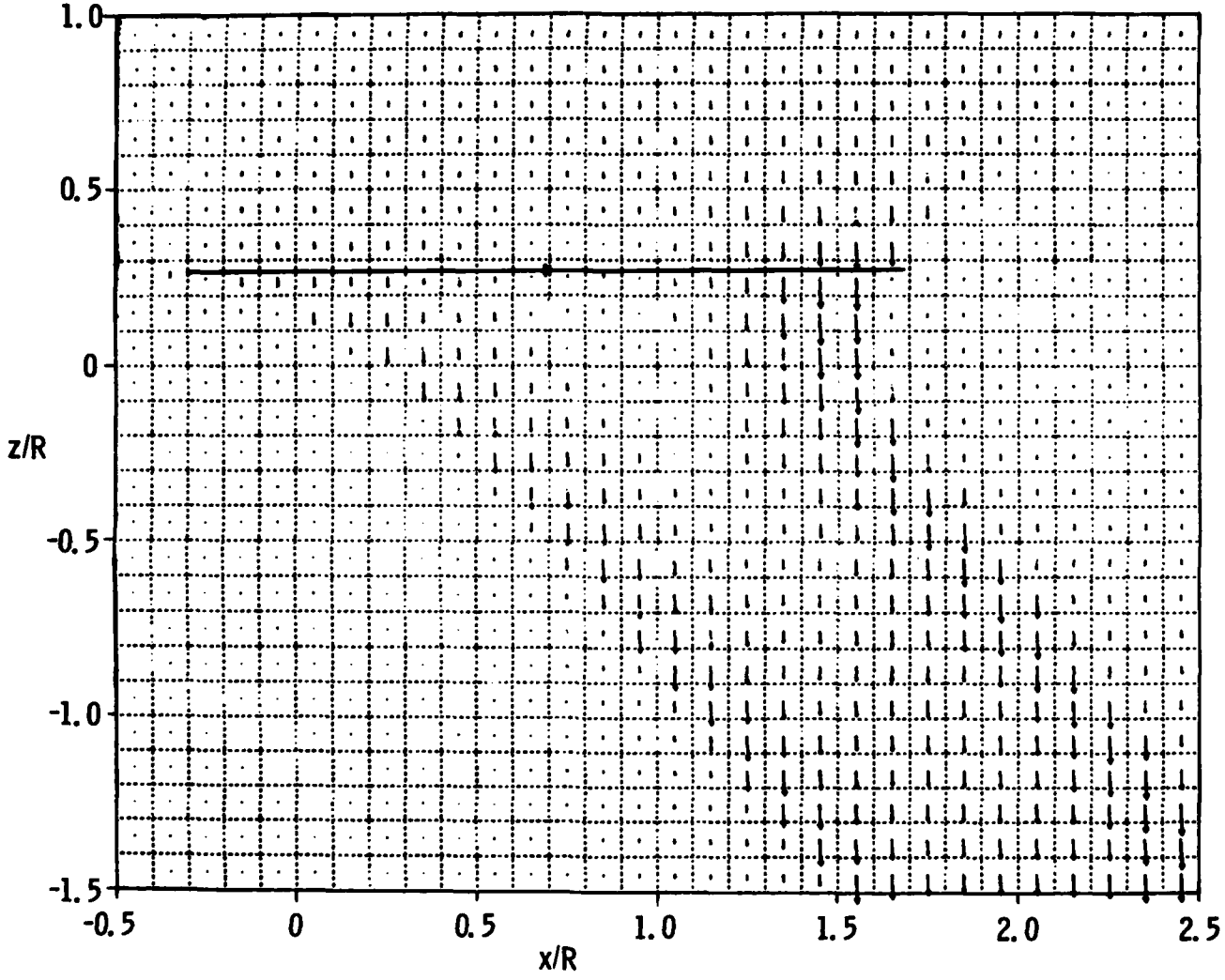

(b) $C_T = 0.0050$.

Figure 6.- Continued.

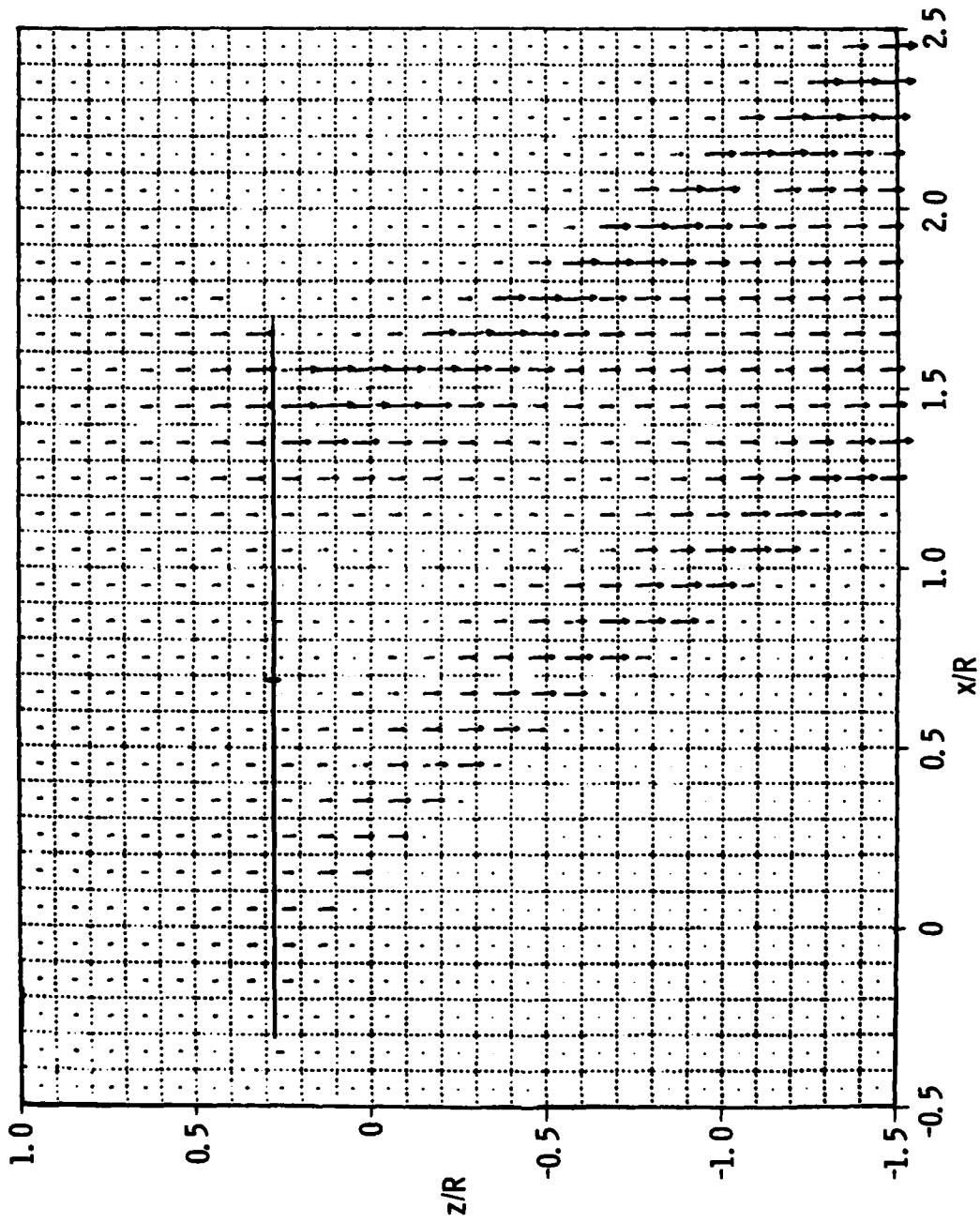

(c) $C_T = 0.0066$.

Figure 6.- Continued.

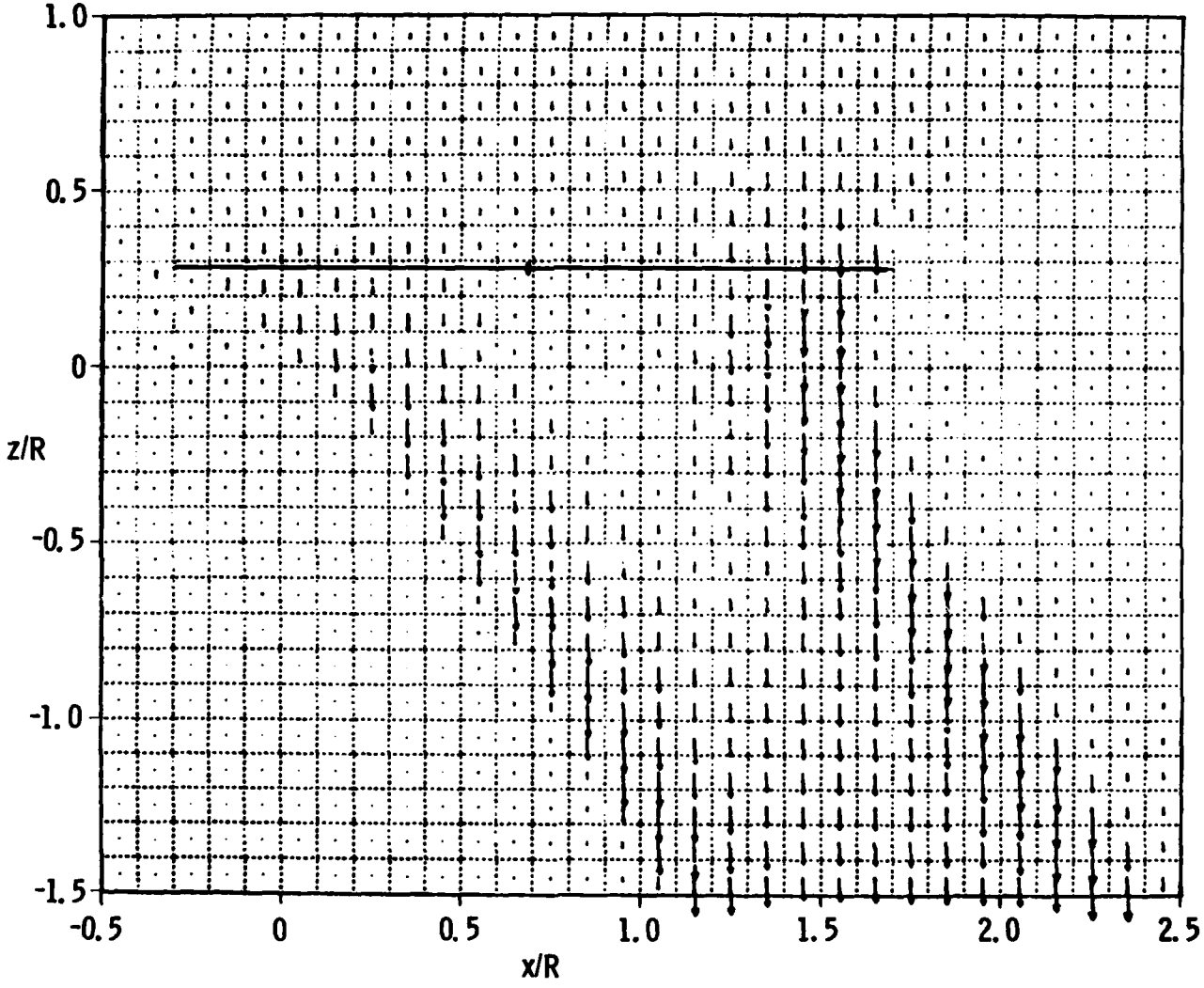

(d) C_T = 0.0082.

Figure 6.- Concluded.

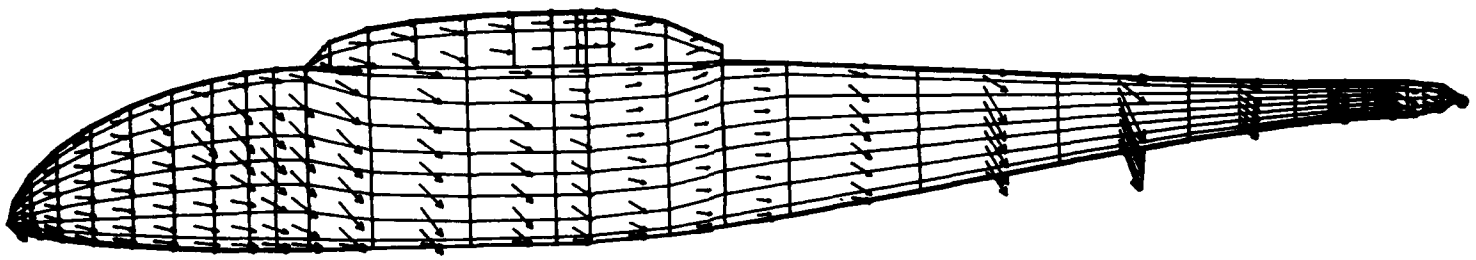

$V/V_\infty = 1.0$

(a) $C_T = 0.0034$.

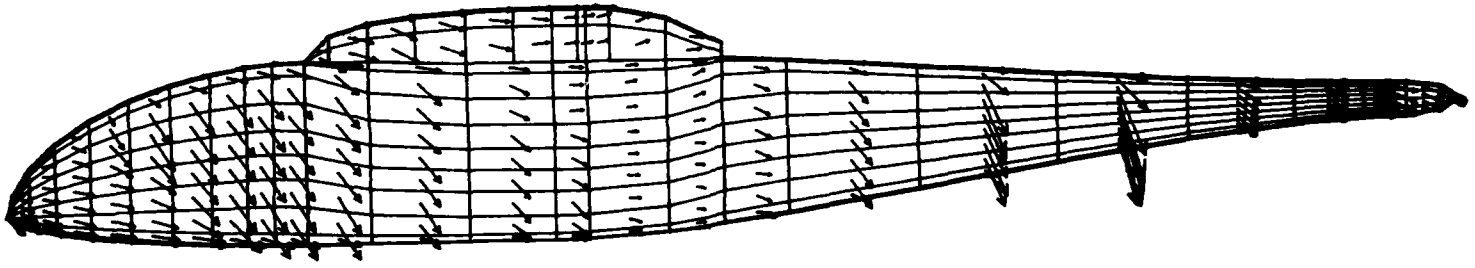

$V/V_\infty = 1.0$

(b) $C_T = 0.0050$.

Figure 7.- Calculated x- and z-components of total velocity on left side of fuselage for $\mu = 0.05$.

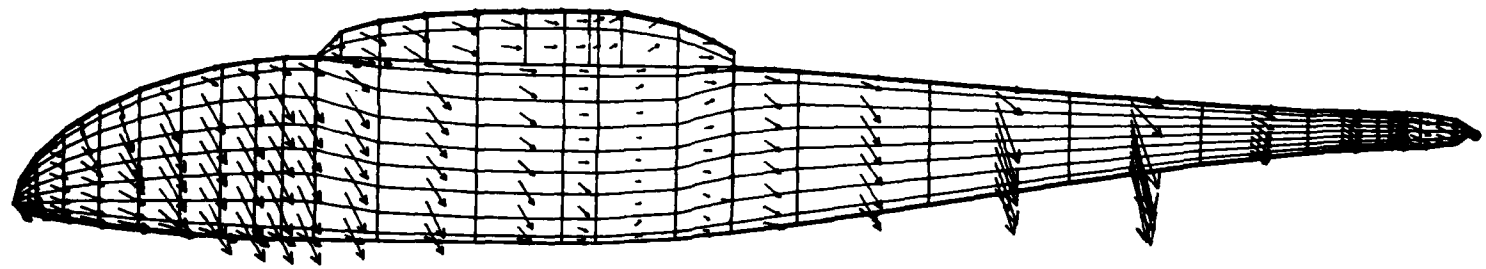

$\rightarrow V/V_\infty = 1.0$

(c) $C_T = 0.0066$.

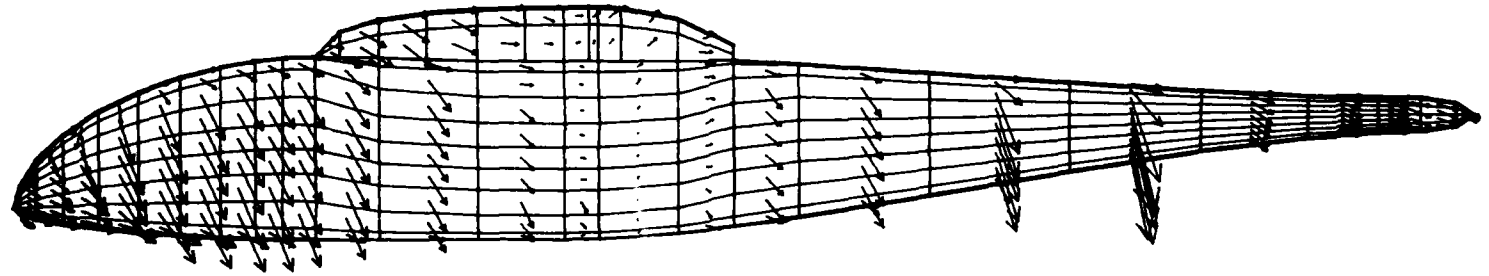

$\rightarrow V/V_\infty = 1.0$

(d) $C_T = 0.0082$.

Figure 7.- Concluded.

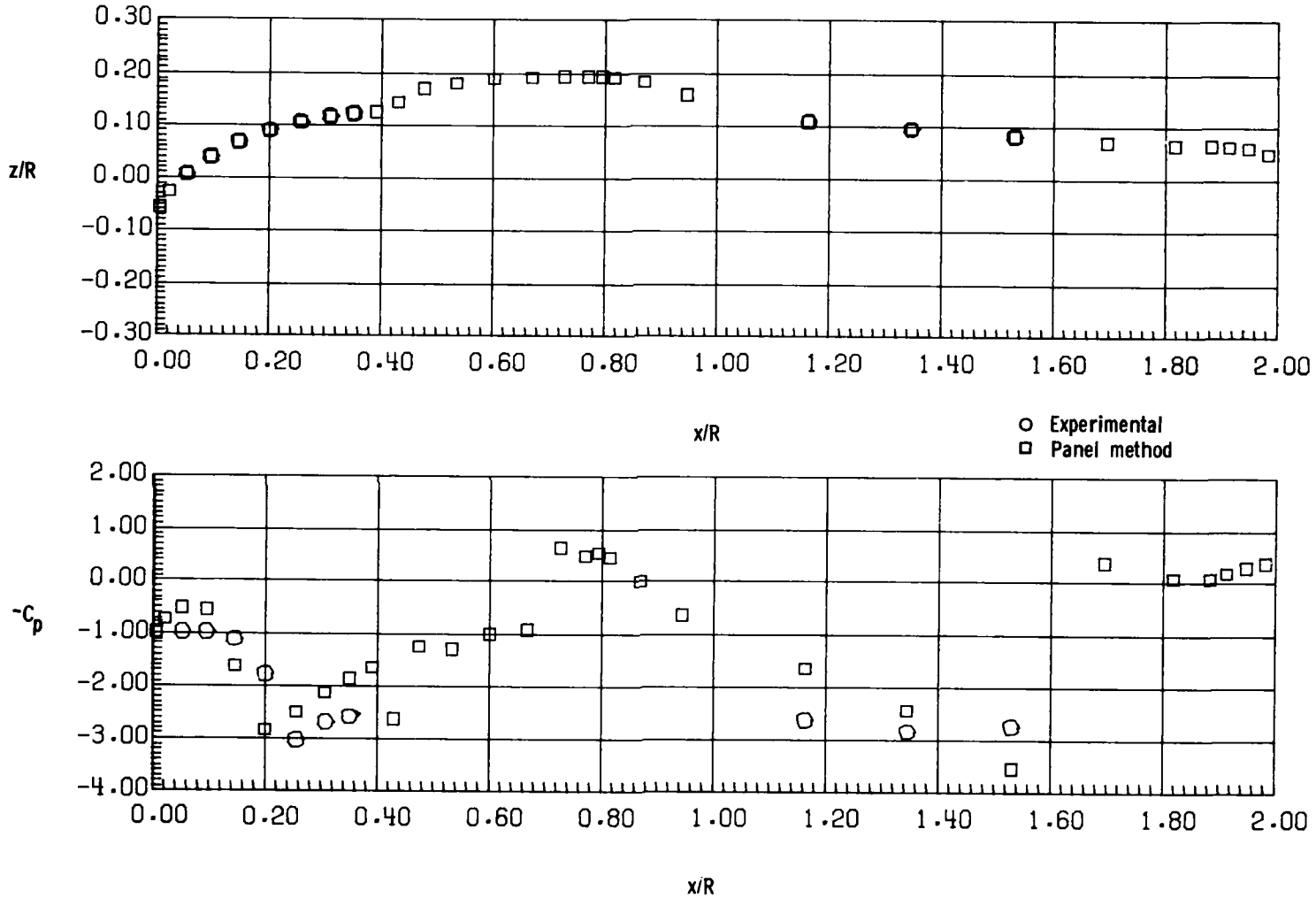

(a) C_T = 0.0033.

Figure 8.- Pressure distribution along top center line of fuselage for μ = 0.05.

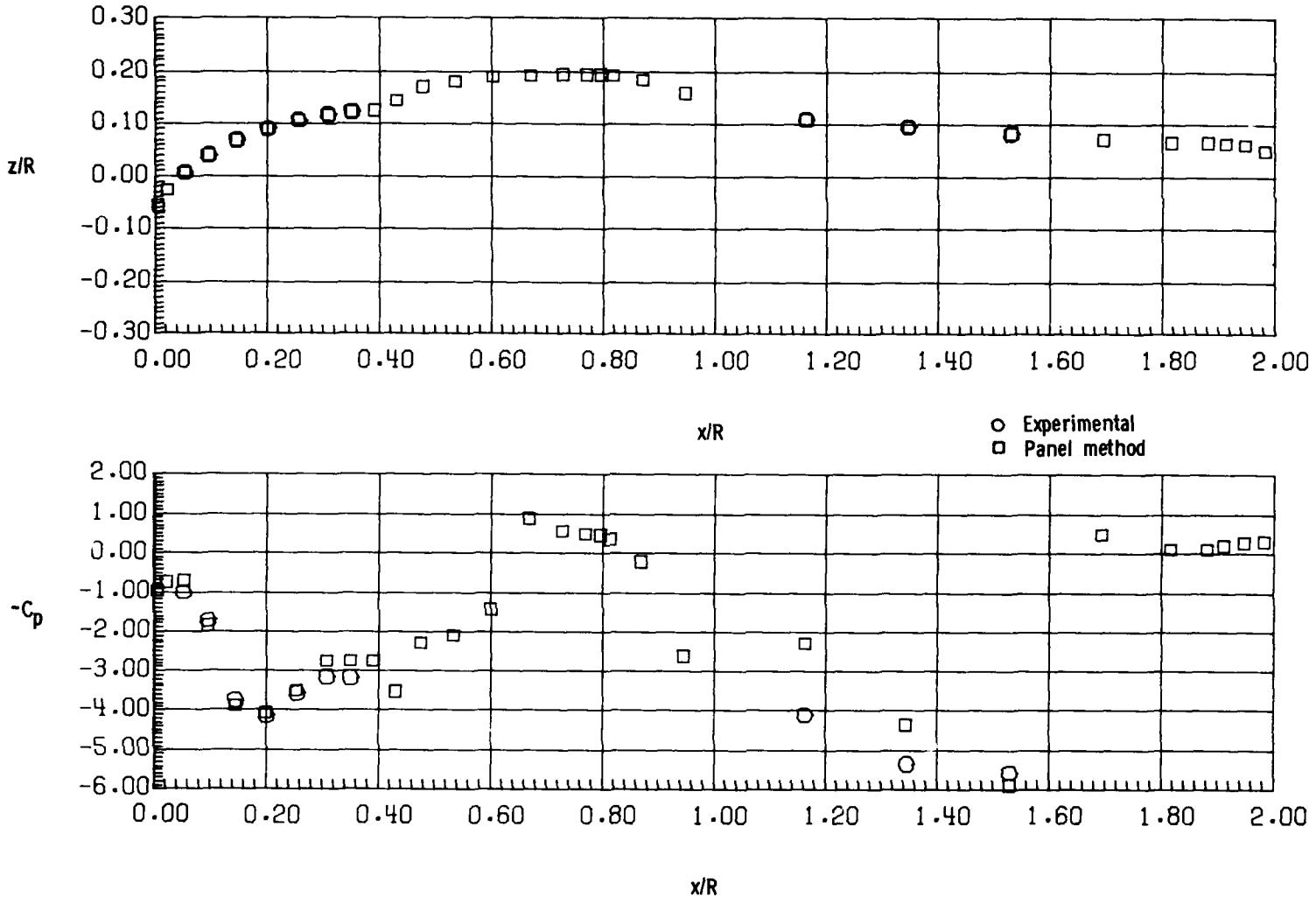

(b) $C_T = 0.0050$.

Figure 8.- Continued.

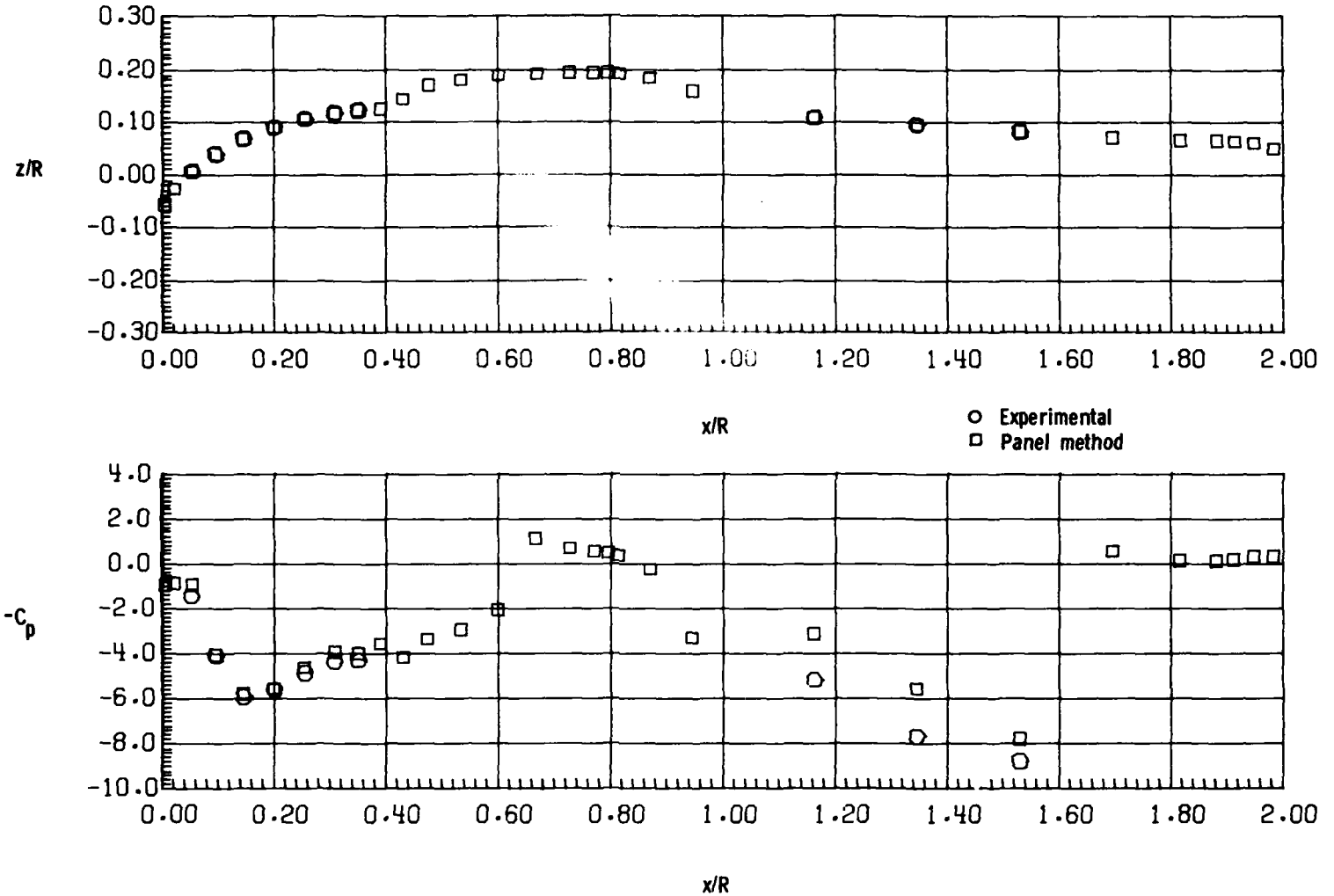

(c) C_T = 0.0066.

Figure 8.- Continued.

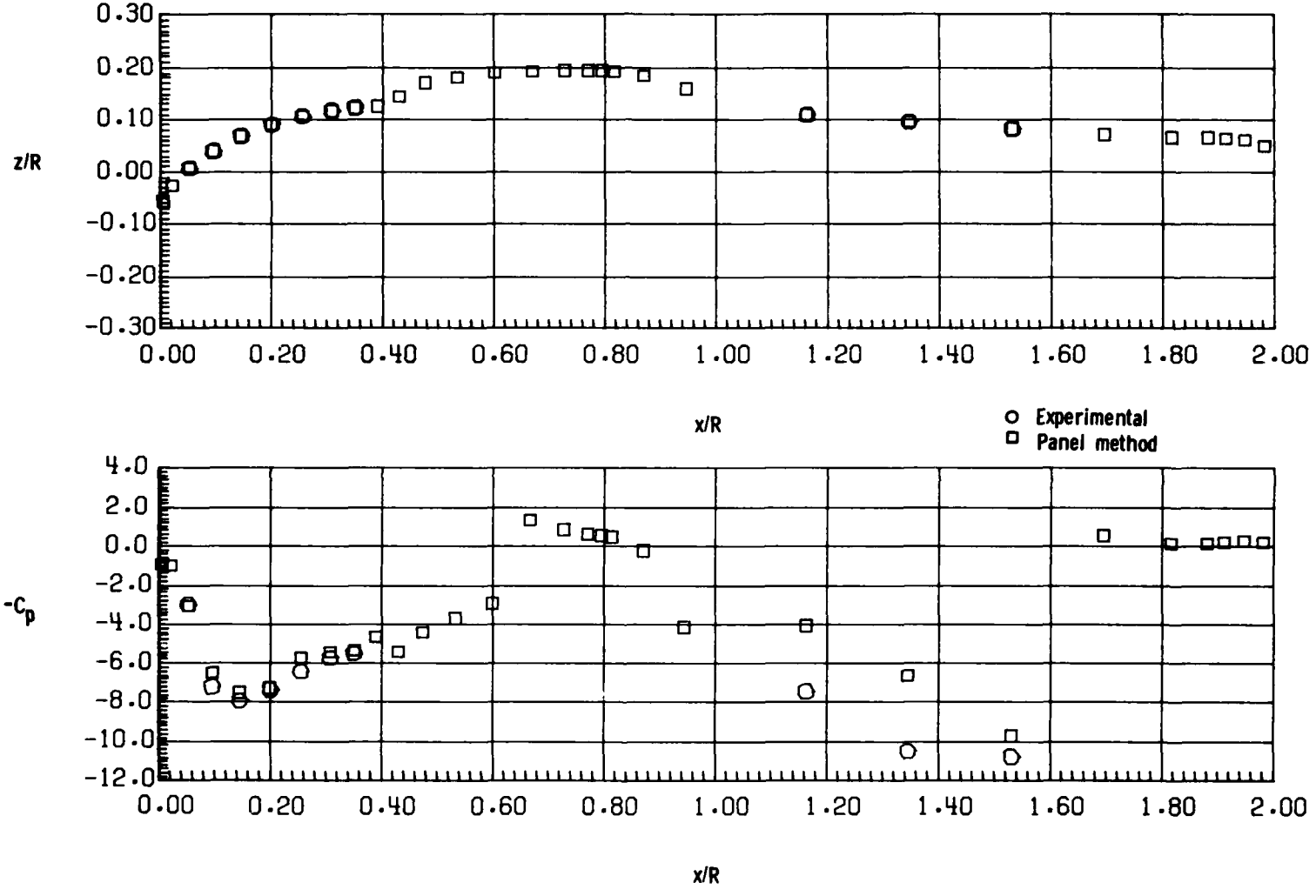

(d) $C_T = 0.0082$.

Figure 8.- Concluded.

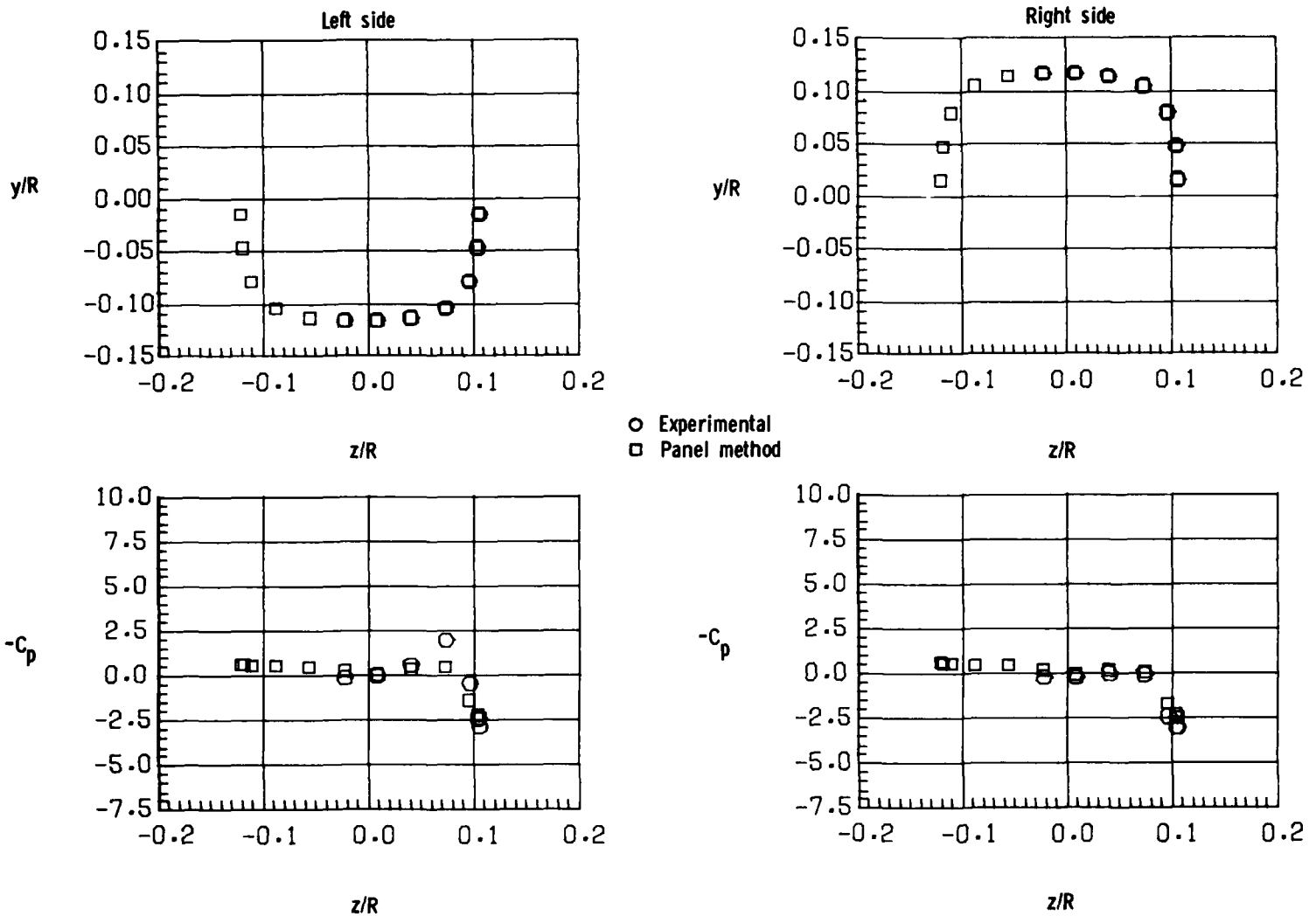

(a) x/R = 0.20; C_T = 0.0034.

Figure 9.- Lateral pressure distributions at four fuselage stations for μ = 0.05.

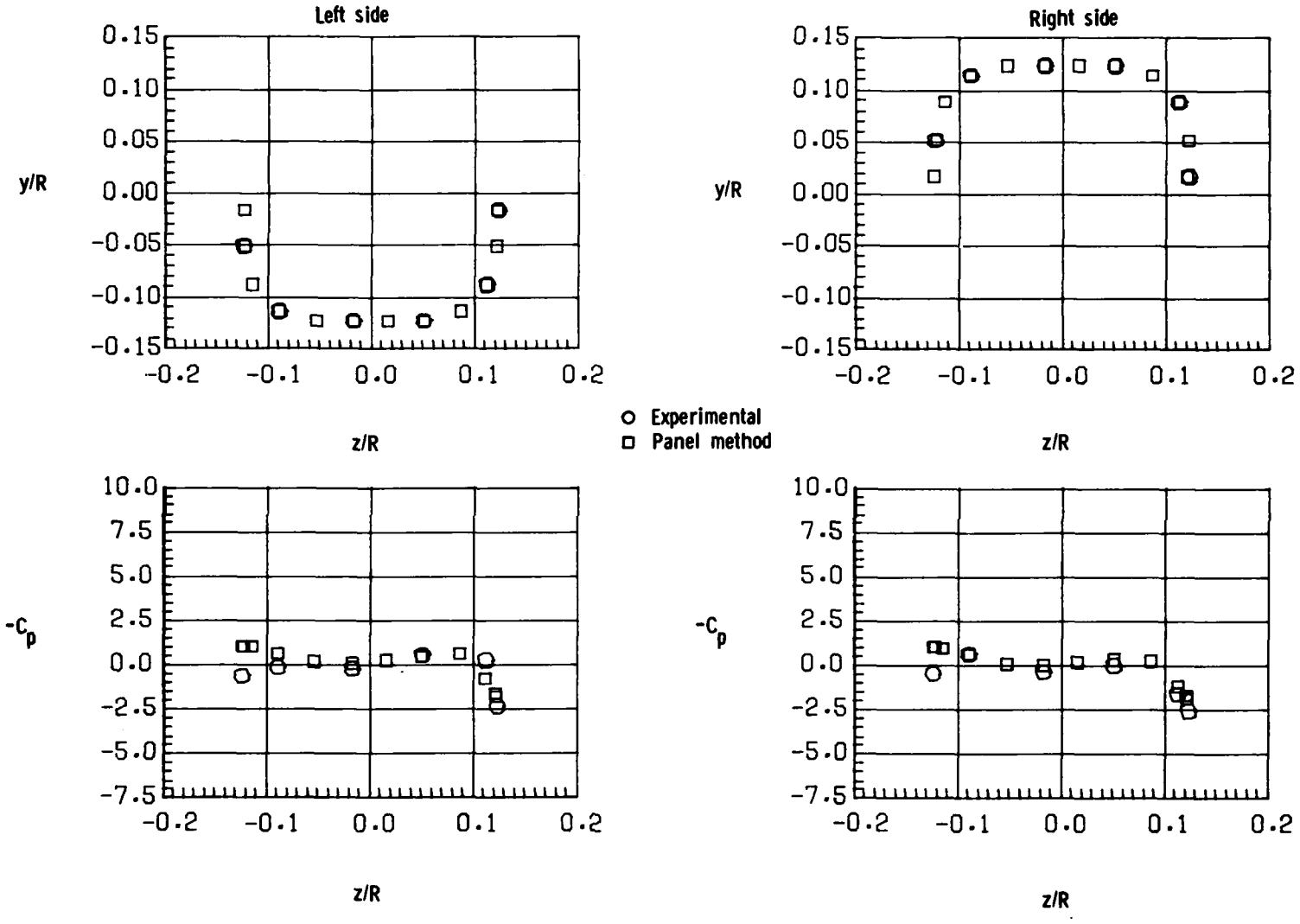

(b) x/R = 0.30; C_T = 0.0034.

Figure 9.- Continued.

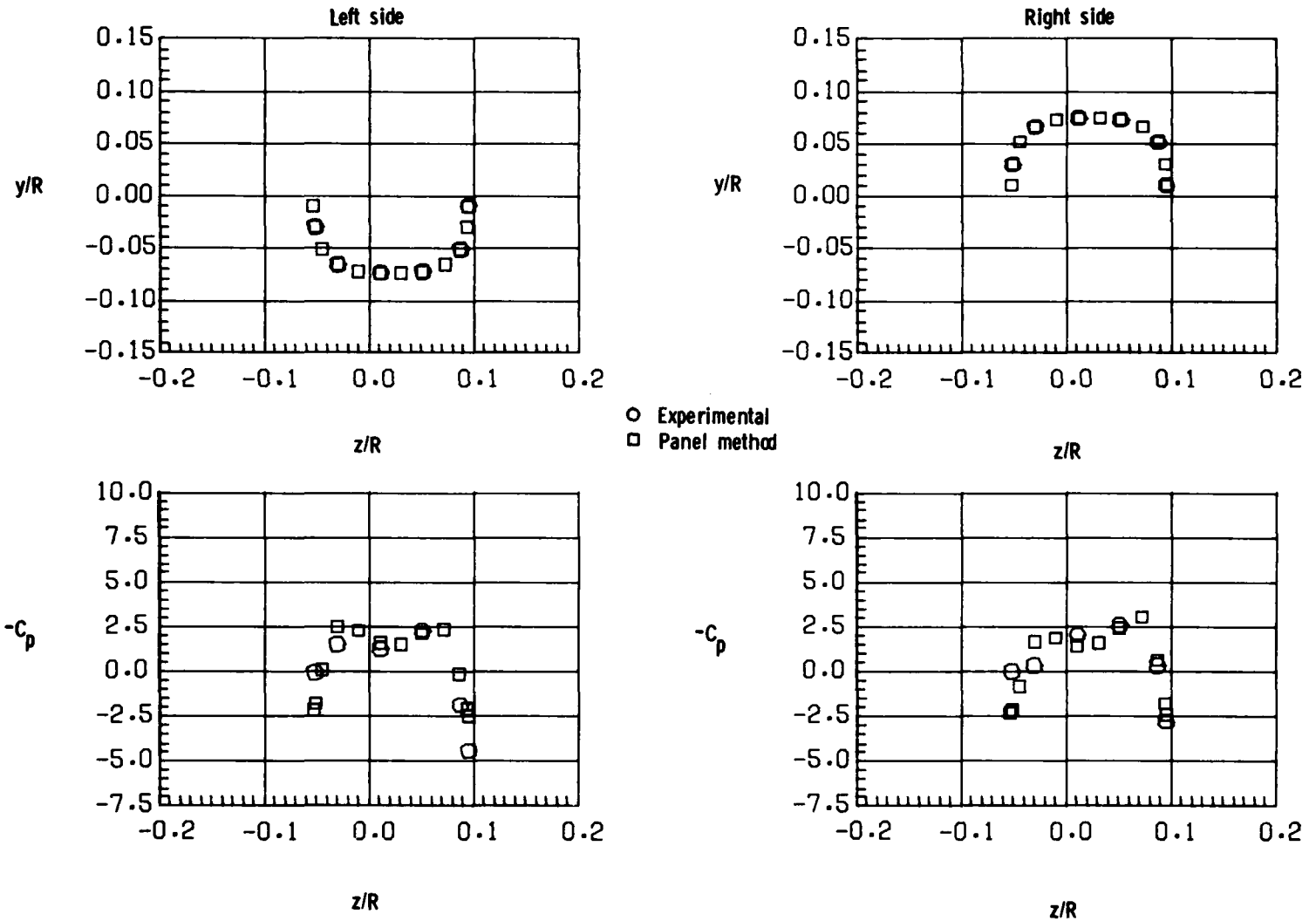

(c) x/R = 1.34; C_T = 0.0034.

Figure 9.- Continued.

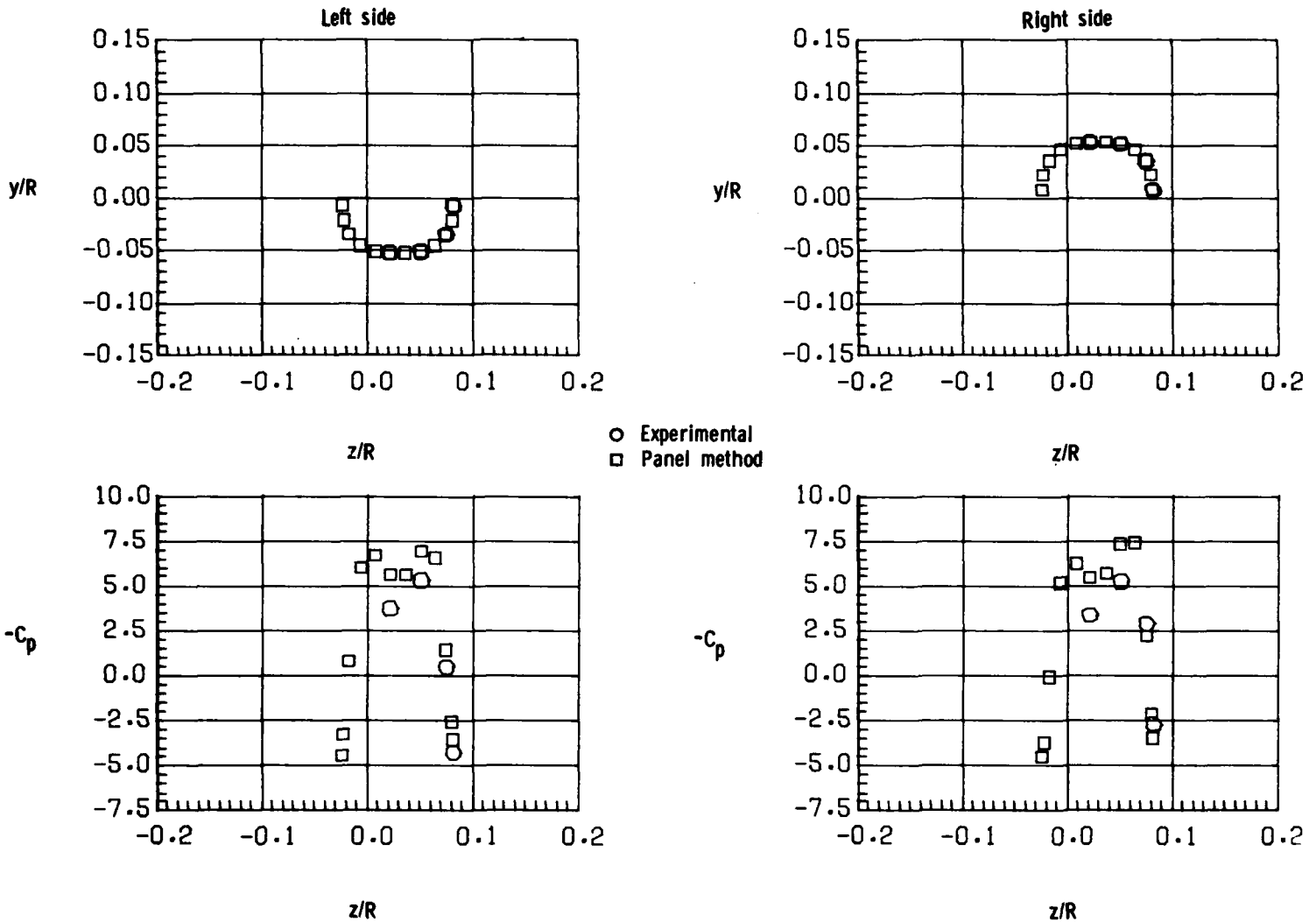

(d) x/R = 1.53; C_T = 0.0034.

Figure 9.- Continued.

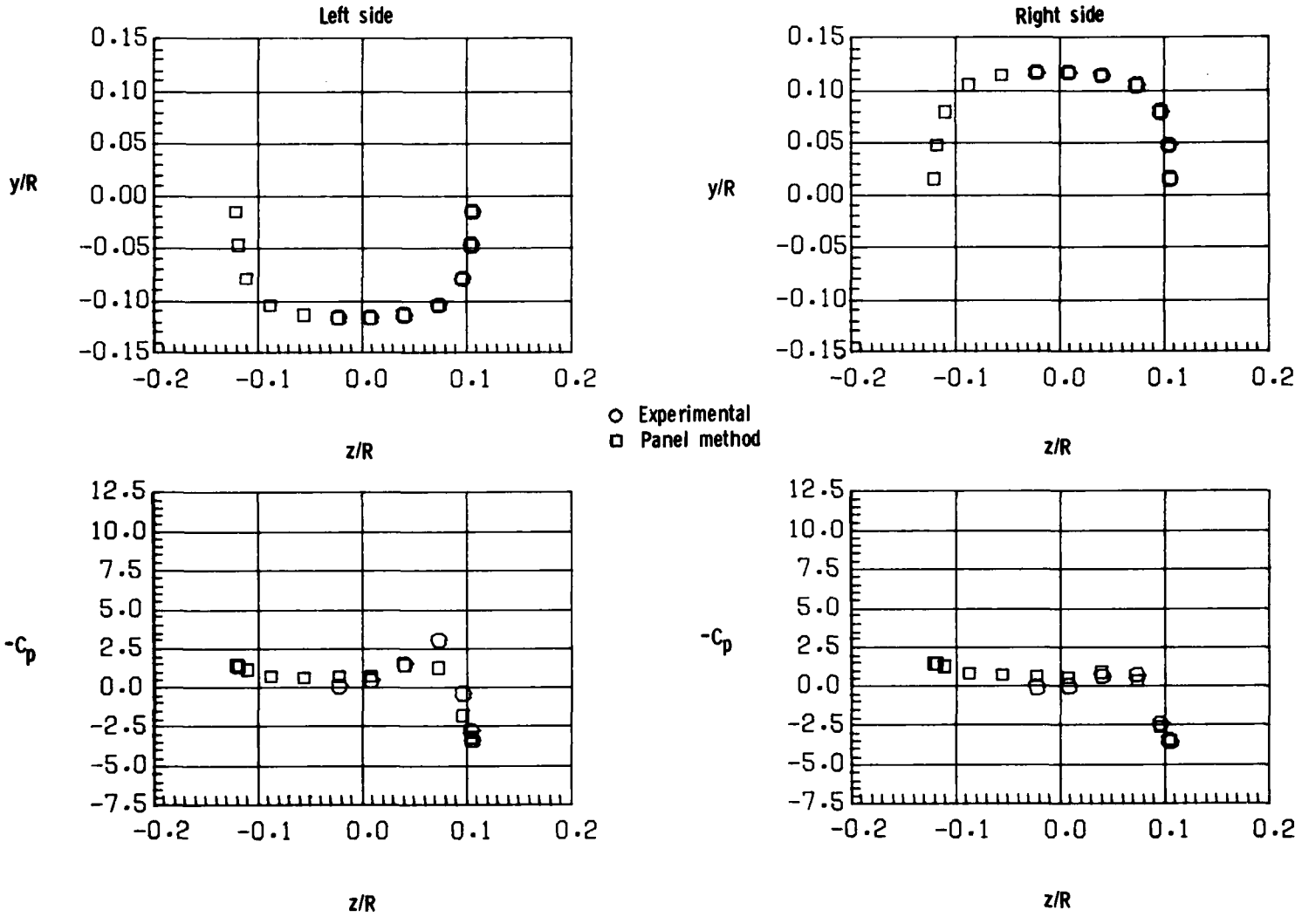

(e) x/R = 0.20; C_T = 0.0050.

Figure 9.- Continued.

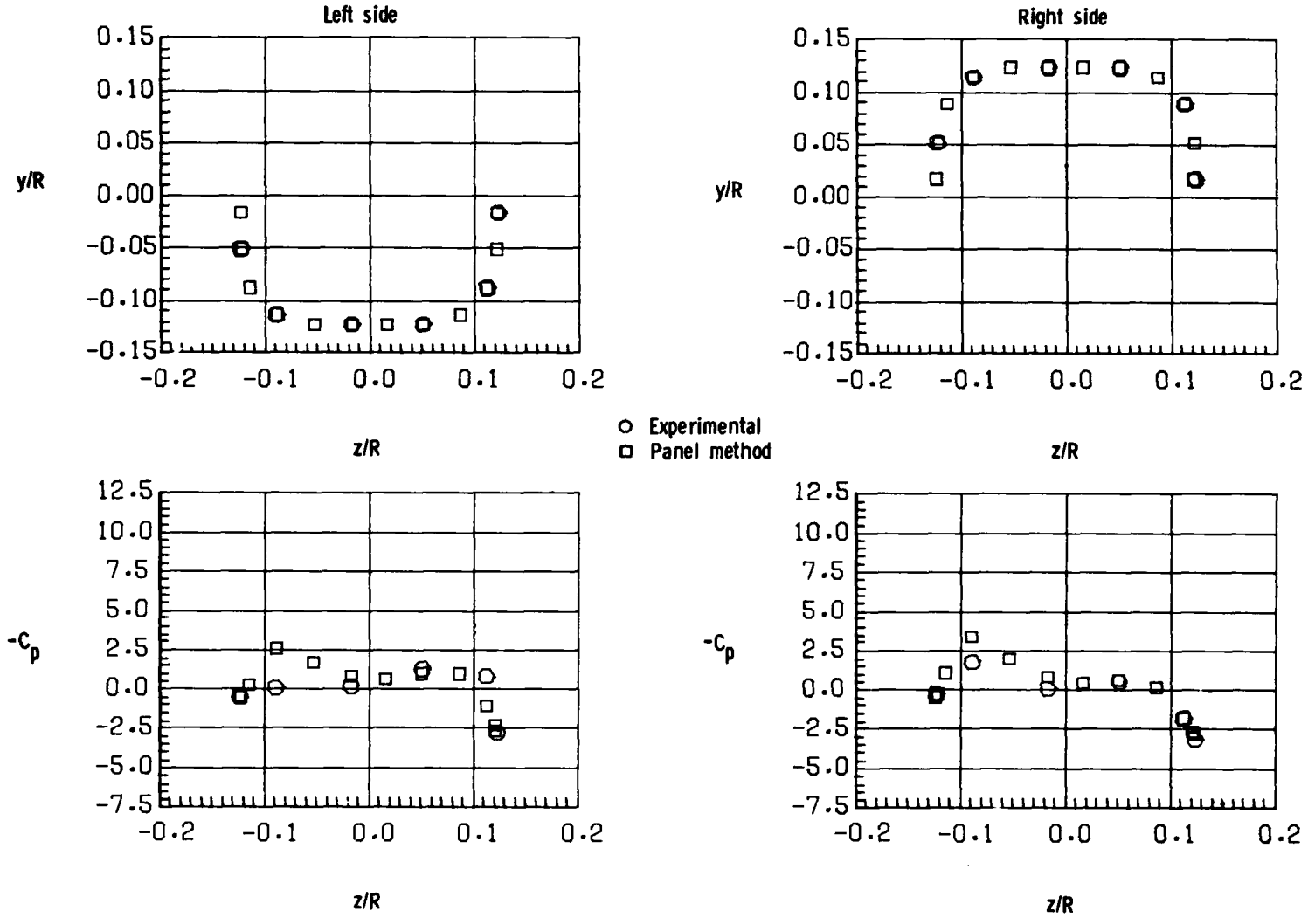

(f) x/R = 0.30; C_T = 0.0050.

Figure 9.- Continued.

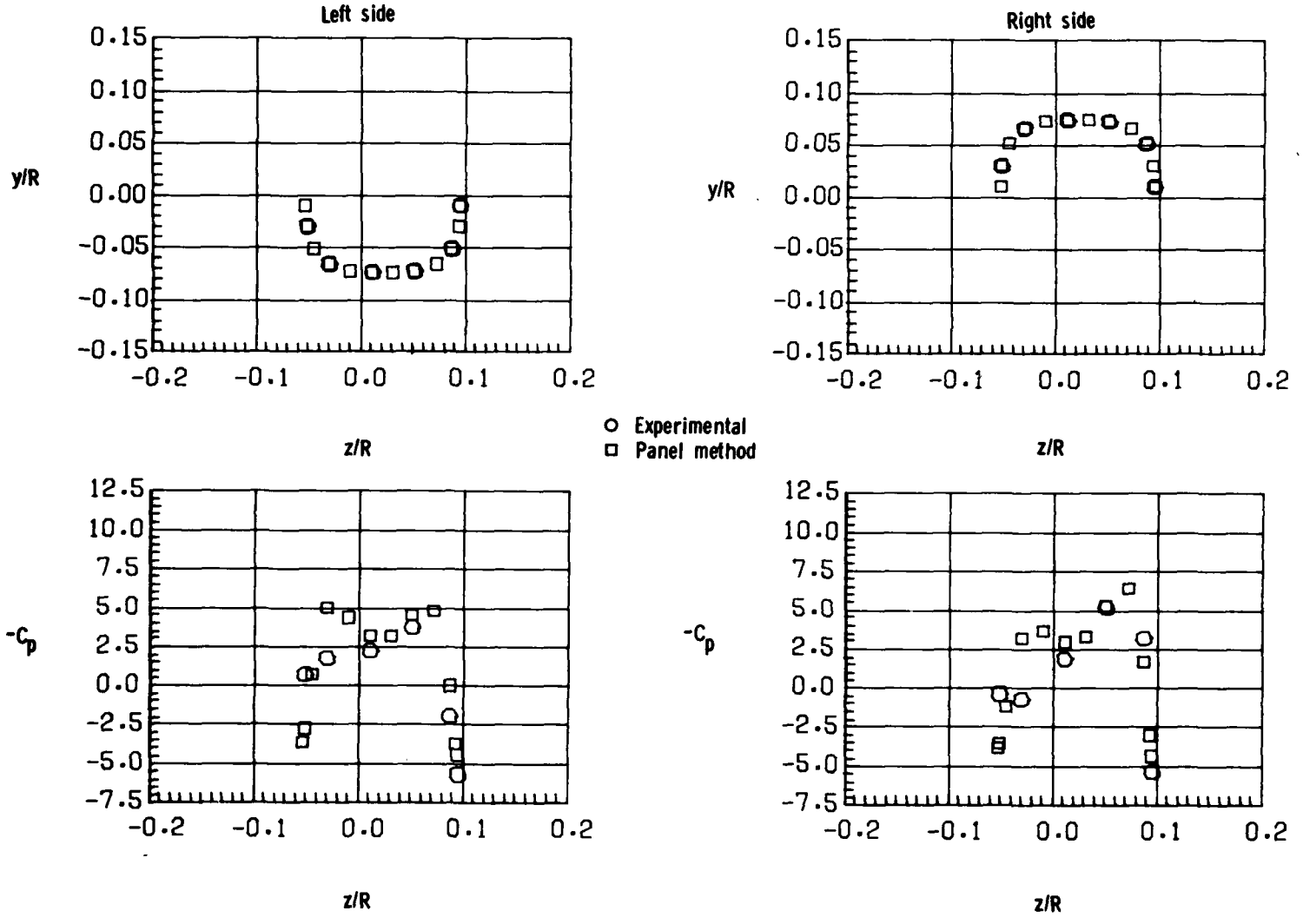

(g) $x/R = 1.34$; $C_T = 0.0050$.

Figure 9.- Continued.

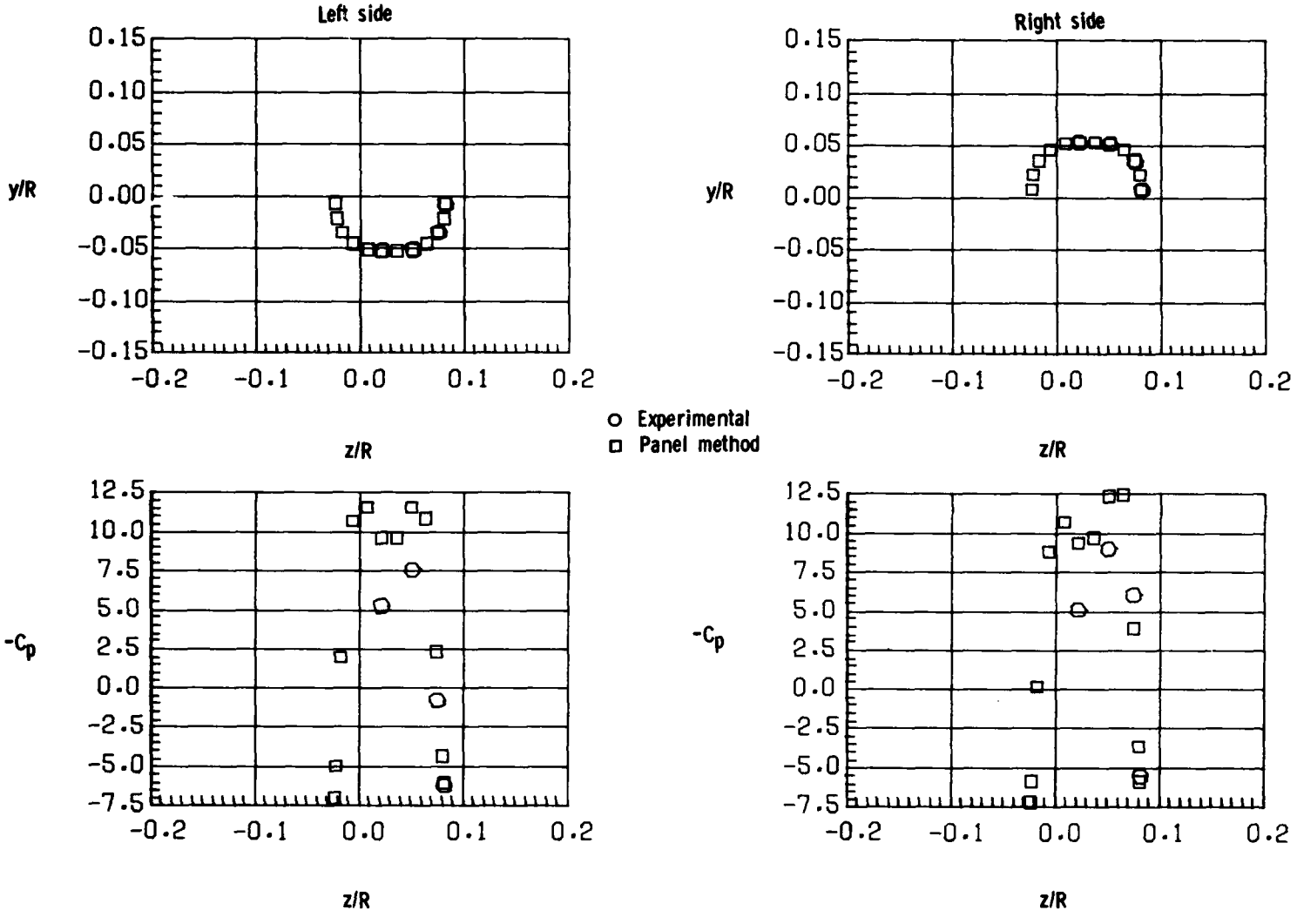

(h) x/R = 1.53; C_T = 0.0050.

Figure 9.- Continued.

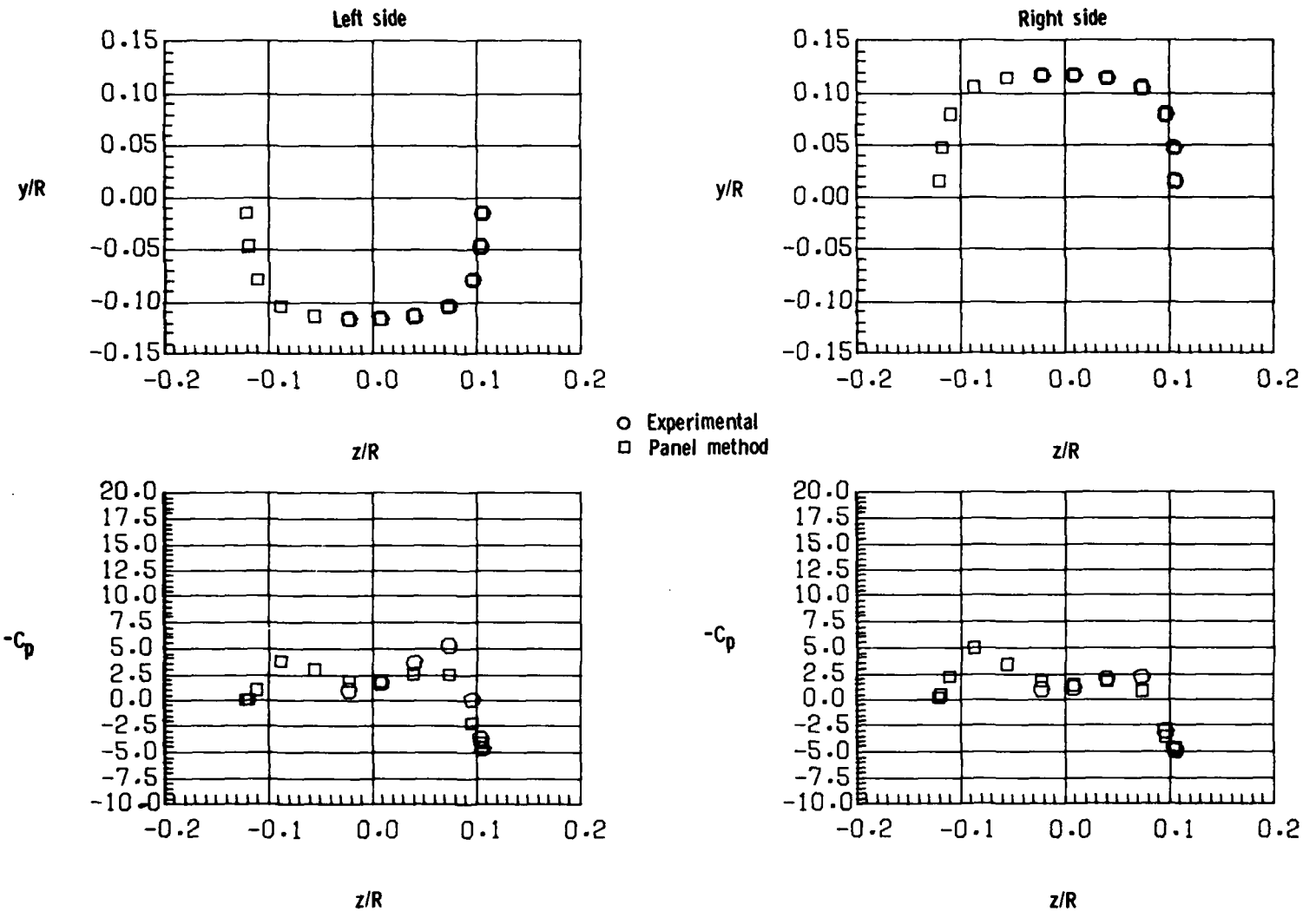

(i) x/R = 0.20; C_T = 0.0066.

Figure 9.- Continued.

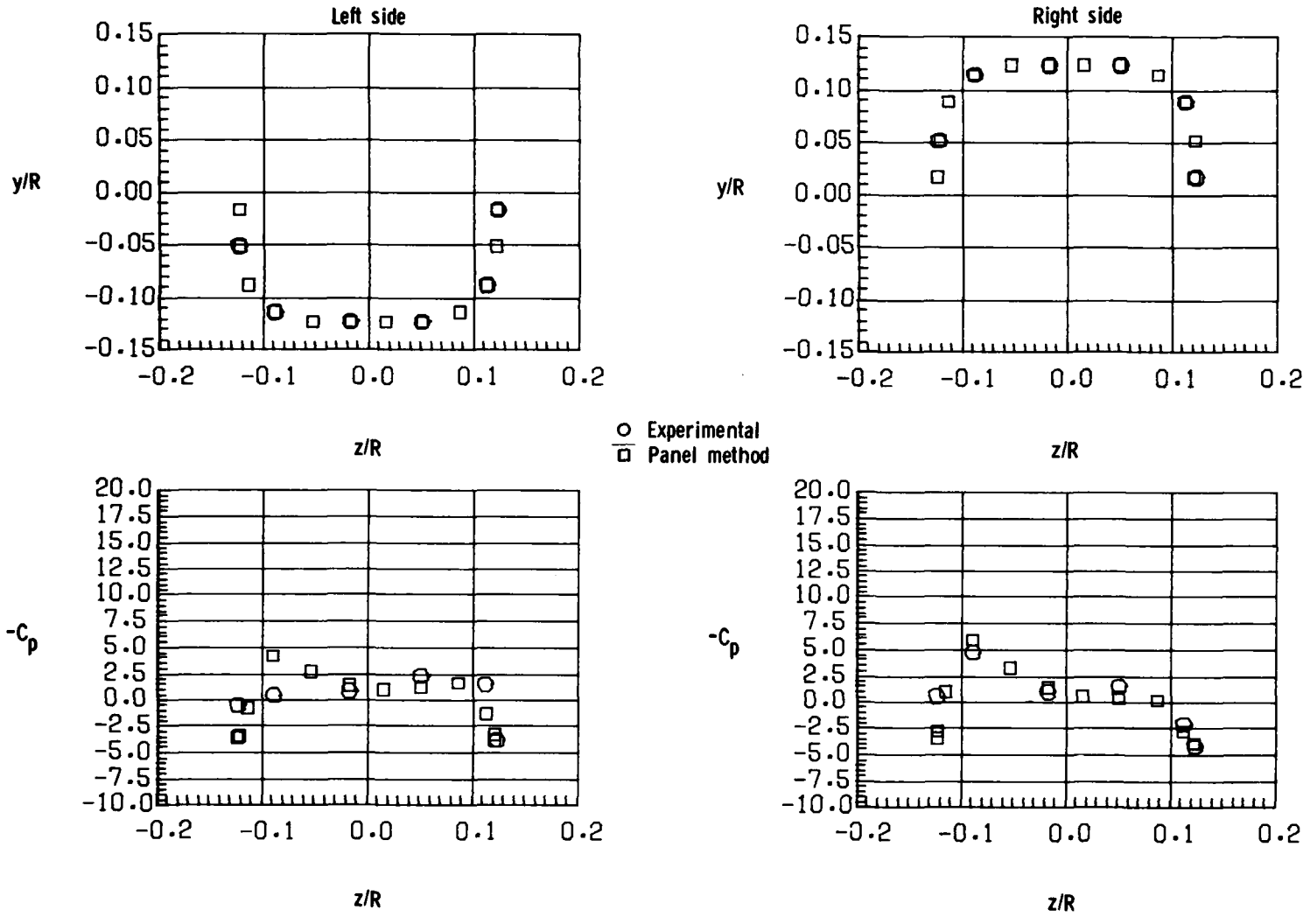

(j) x/R = 0.30; C_T = 0.0066.

Figure 9.- Continued.

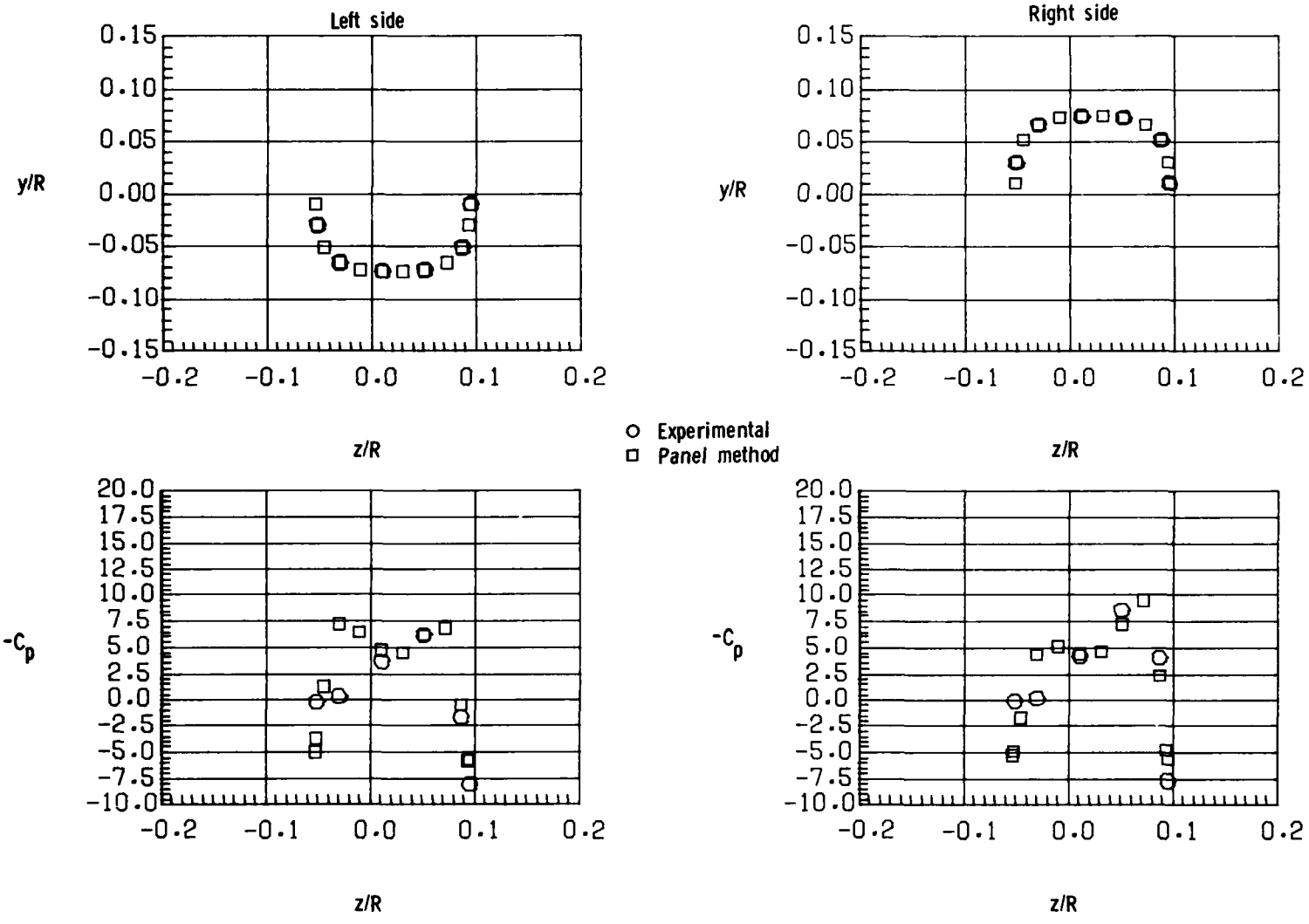

(k) x/R = 1.34; C_T = 0.0066.

Figure 9.- Continued.

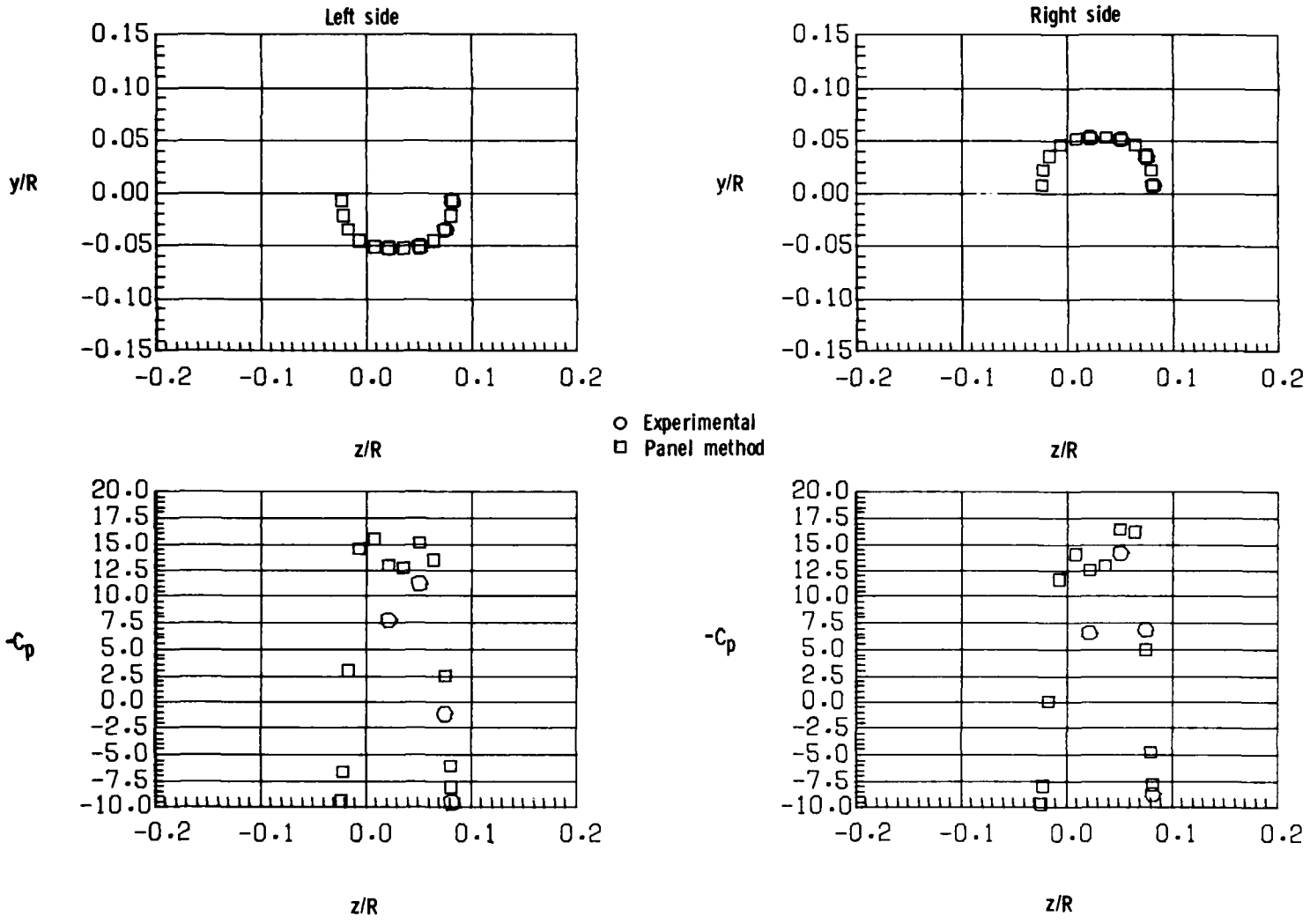

(l) x/R = 1.53; C_T = 0.0066.

Figure 9.- Continued.

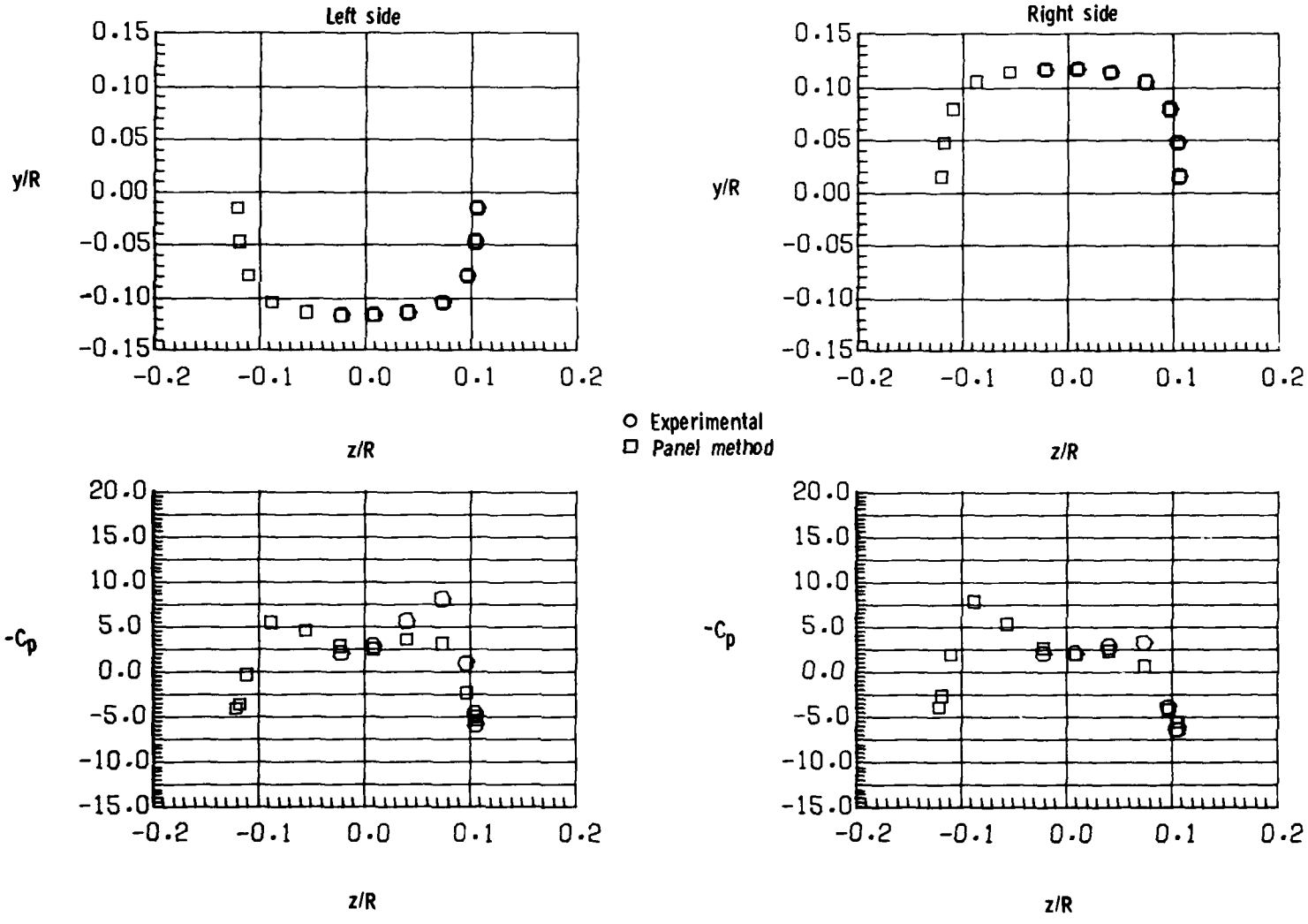

(m) x/R = 0.20; C_T = 0.0082.

Figure 9.- Continued.

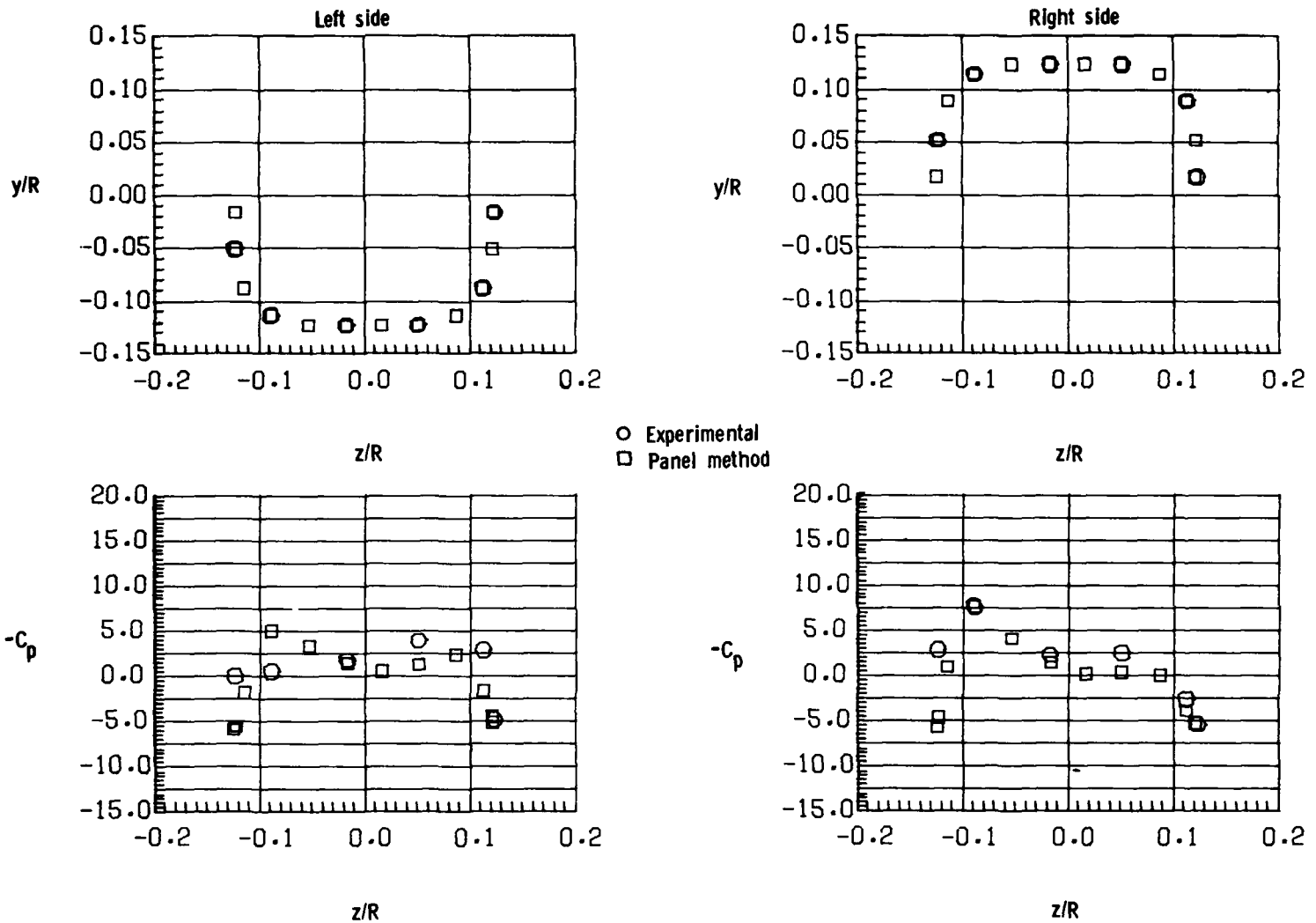

(n) x/R = 0.30; C_T = 0.0082.

Figure 9.- Continued.

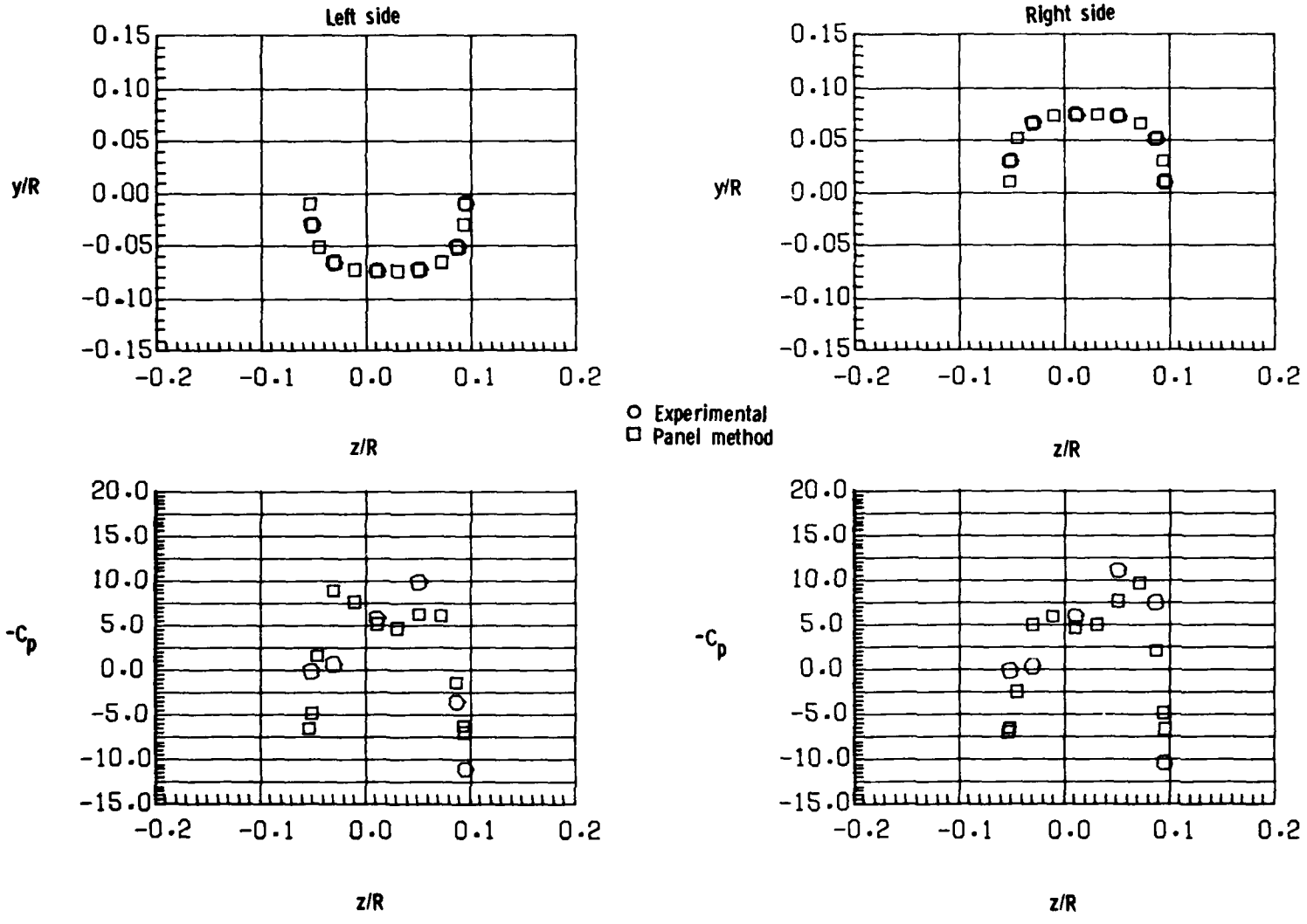

(o) x/R = 1.34; C_T = 0.0082.

Figure 9.- Continued.

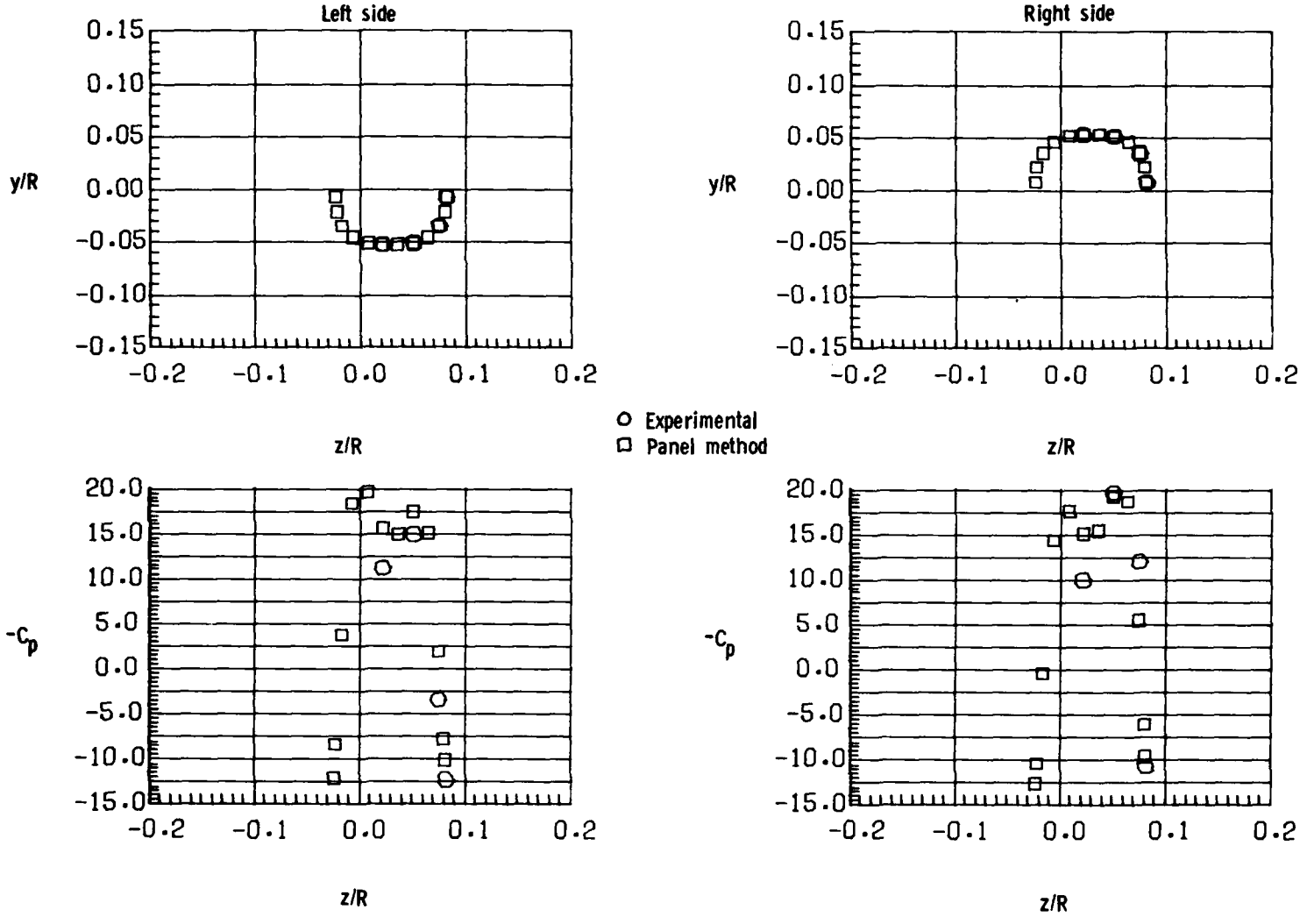

(p) x/R = 1.53; C_T = 0.0082.

Figure 9.- Concluded.

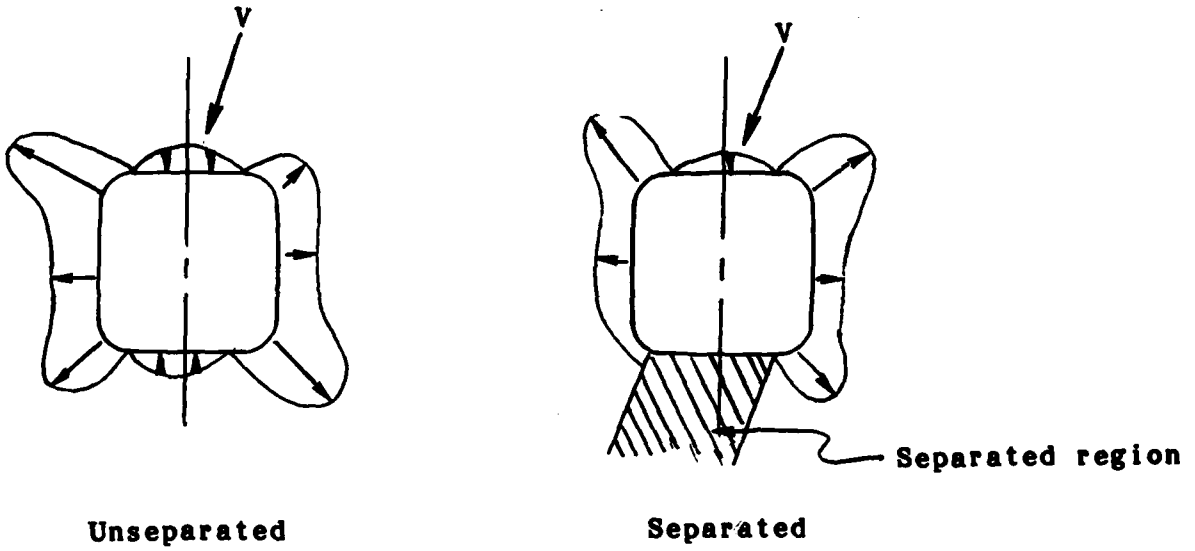

Figure 10.- Separation and swirl effects on fuselage cross-section pressure distribution.

1. Report No.	2. Government Accession No.	3. Recipient's Catalog No.
NASA TP-1656 / AVRADCOM TR 80-B-3	AD-A085 968	

4. Title and Subtitle

DEVELOPMENT AND VALIDATION OF A COMBINED ROTOR-FUSELAGE INDUCED FLOW-FIELD COMPUTATIONAL METHOD

5. Report Date	6. Performing Organization Code
June 1980	

7. Author(s)

Carl E. Freeman

8. Performing Organization Report No.	10. Work Unit No.	11. Contract or Grant No.
L-13363	505-42-23-03	

9. Performing Organization Name and Address

NASA Langley Research Center
and
Structures Laboratory
AVRADCOM Research and Technology Laboratories
Hampton, VA 23665

12. Sponsoring Agency Name and Address

National Aeronautics and Space Administration
Washington, DC 20546
and
U.S. Army Aviation Research and Development Command
St. Louis, MO 63166

13. Type of Report and Period Covered	14. Army Project No.
Technical Paper	1L161102AH45-A

15. Supplementary Notes

Carl E. Freeman: Structures Laboratory, AVRADCOM, Research and Technology Laboratories.

16. Abstract

A potential-flow panel method has been modified to calculate the effects of a rotor wake on the time-averaged surface pressure and velocity distributions on a helicopter fuselage. The rotor-induced velocities are calculated by using a vortex-tube wake model. The calculated pressure distributions are found to compare well with experimental data obtained from tests of a wind-tunnel model.

17. Key Words (Suggested by Author(s))	18. Distribution Statement
Rotor wake Computational aerodynamics Helicopter aerodynamics	Unclassified - Unlimited Subject Category 02

19. Security Classif. (of this report)	20. Security Classif. (of this page)	21. No. of Pages	22. Price*
Unclassified	Unclassified	58	$5.25

*For sale by the National Technical Information Service, Springfield, Virginia 22161

NASA-Langley, 1980

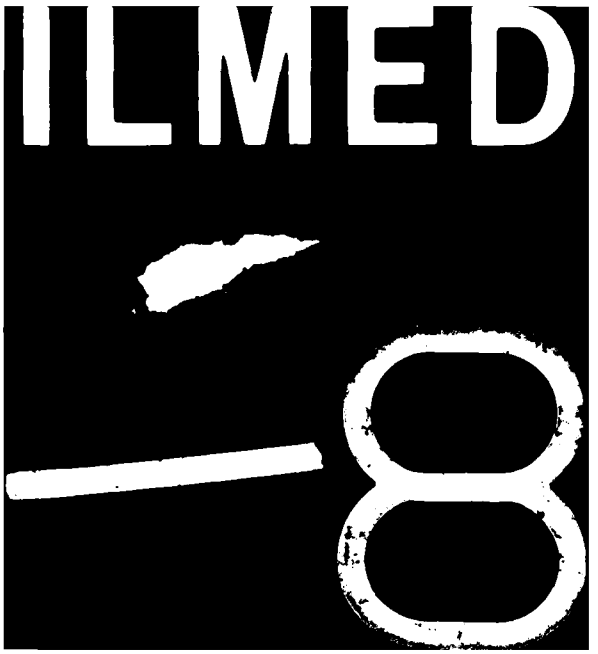
ILMED
18